hydrology

MDPI

Article

Conceptual and Mathematical Modeling of a Coastal Aquifer in Eastern Delta of R. Nestos (N. Greece)

Ioannis Gkiougkis [1,*], Christos Pouliaris [2], Fotios-Konstantinos Pliakas [1], Ioannis Diamantis [1] and Andreas Kallioras [2]

[1] Department of Civil Engineering, Democritus University of Thrace, 67100 Xanthi, Greece; fpliakas@civil.duth.gr (F.-K.P.); jdiam@civil.duth.gr (I.D.)
[2] School of Mining & Metallurgical Engineering, National Technical University of Athens, 15780 Athens, Greece; pouliaris@metal.ntua.gr (C.P.); kallioras@metal.ntua.gr (A.K.)
* Correspondence: jgiougis@civil.duth.gr

Abstract: In this paper, the development of the conceptual and groundwater flow model for the coastal aquifer system of the alluvial plain of River Nestos (N. Greece), that suffers from seawater intrusion due to over-pumping for irrigation, is analyzed. The study area is a typical semi-arid hydrogeologic environment, composed of a multi-layer granular aquifers that covers the eastern coastal delta system of R. Nestos. This study demonstrates the results of a series of field measurements (such as geophysical surveys, hydrochemical and isotopical measurements, hydro-meteorological data, land use, irrigation schemes) that were conducted during the period 2009 to 2014. The synthesis of the above resulted in the development of the conceptual model for this aquifer system, that formed the basis for the application of the mathematical model for simulating groundwater flow. The mathematical modeling was achieved using the finite difference method after the application of the USGS code MODFLOW-2005.

Keywords: seawater intrusion; coastal aquifer management; conceptual model; groundwater flow simulation; MODFLOW

Citation: Gkiougkis I.; Pouliaris C.; Pliakas F.; Diamantis I.; Kallioras A. Conceptual and Mathematical Modeling of a Coastal Aquifer in Eastern Delta of R. Nestos (N. Greece). *Hydrology* **2021**, *8*, 23. https://doi.org/10.3390/hydrology8010023

Received: 17 December 2020
Accepted: 25 January 2021
Published: 29 January 2021

1. Introduction

Coastal aquifer systems are considered a water resource reservoir of ample importance, since almost 50% of global population lives within a zone of several kilometers away from the coast and therefore depend largely on them for their water supply. However, these environmental systems are considered hydrologically sensitive as they are vulnerable to salinization due to seawater intrusion, as a result of overexploitation. The aforementioned argument is proved by numerous case studies which are reported in scientific literature [1–8], proving that ecosystem services of coastal aquifers have become limited. The above problem becomes even more pronounced in semi-arid and arid climatic zones, such as the conditions within the Circum-Mediterranean [9–45], where limited groundwater resources may pose serious socio-economic impacts.

Based on the above, it can be realized that sustainable use of groundwater is considered a key issue for the optimized management of water resources of these systems, which in turn relies solely on extensive monitoring of hydrologic processes. The latter, is usually conducted within a model-driven approach, as it usually provides a mathematical model with input data in order to predict the future response of the aquifer under different optimizations scenarios.

The investigation of such complex physical systems usually demands a series of field measurements for the development of a reliable conceptual model, which in turn will result in a reliable mathematical model. It is also argued that the more accurate the conceptual model, the less efforts are needed for the application of the mathematical model. Accurate conceptual model is directly related to a thorough investigation of the natural system involving subsurface investigations (groundwater well logging, geophysical investigations, pumping tests), hydrological (groundwater level monitoring, surface and unsaturated zone studies) and hydrochemical measurements (groundwater sampling and analyses).

This paper describes the use of a complete set of field hydrogeological investigations for the analysis of a coastal aquifer system in semi-arid conditions, in order to form the basis for the development of a conceptual aquifer model. Then, based on the above, the research involved the application of a mathematical groundwater flow simulation model.

2. Location of the Study Area

The research area is surrounded by Nestos river on the west and by the Aegean Sea on the south (Figure 1). The broader region morphology, on the south and south-east, is identified by low relief and some shallow pits, thus creating minor ponds, that are fragment of the eastern Nestos River delta wetland. The research area is mainly coved by clay, sandy clay, sand and in some cases pebbles (Figure 2). Nestos River stands dominant as the most significant surface water body of this region. It is situated on the west of the research area, and at the same time, it is considered to be one of the major recharge source of freshwater for the inshore unconfined aquifer of the research area [46–48]. Laspias stream is situated along the eastern boundaries of the research area where the degraded industrial and sewage treatment effluents are discharged. The composite image of Figure 1, shows: (i) the monitoring network of groundwater wells of the study area, (ii) the location of geoelectrical sounding measurements sites along the boundary conditions in conjunction with the resulted geological sections, (iii) axes of geological material graduation, (iv) locations of the upper layer of sand-gravel material (thickness: 5–20 m) and locations of upper layer of clay-sand material (thickness: 15–20 m).

The research area is part of the National Park of Eastern Macedonia—Thrace, that was founded in 2008 and included the already protected areas of Nestos Delta, Vistonidas Lagoon, Ismarida Lagoon and their wider area. The study area (Figure 2) faces serious environmental degradation due to:

- The annual decrease of groundwater level of phreatic aquifers due to reduction of natural recharge with fresh water.
- The seawater intrusion, occurring on surface water bodies as well as on groundwater aquifers.
- The quality degradation of fresh water from different sources such as: applied fertilizers and pesticides, irrigation return flows and disposal of municipal and industrial waste.
- The use of wetlands for grazing and fishing.
- The rural development of the coastal zone.

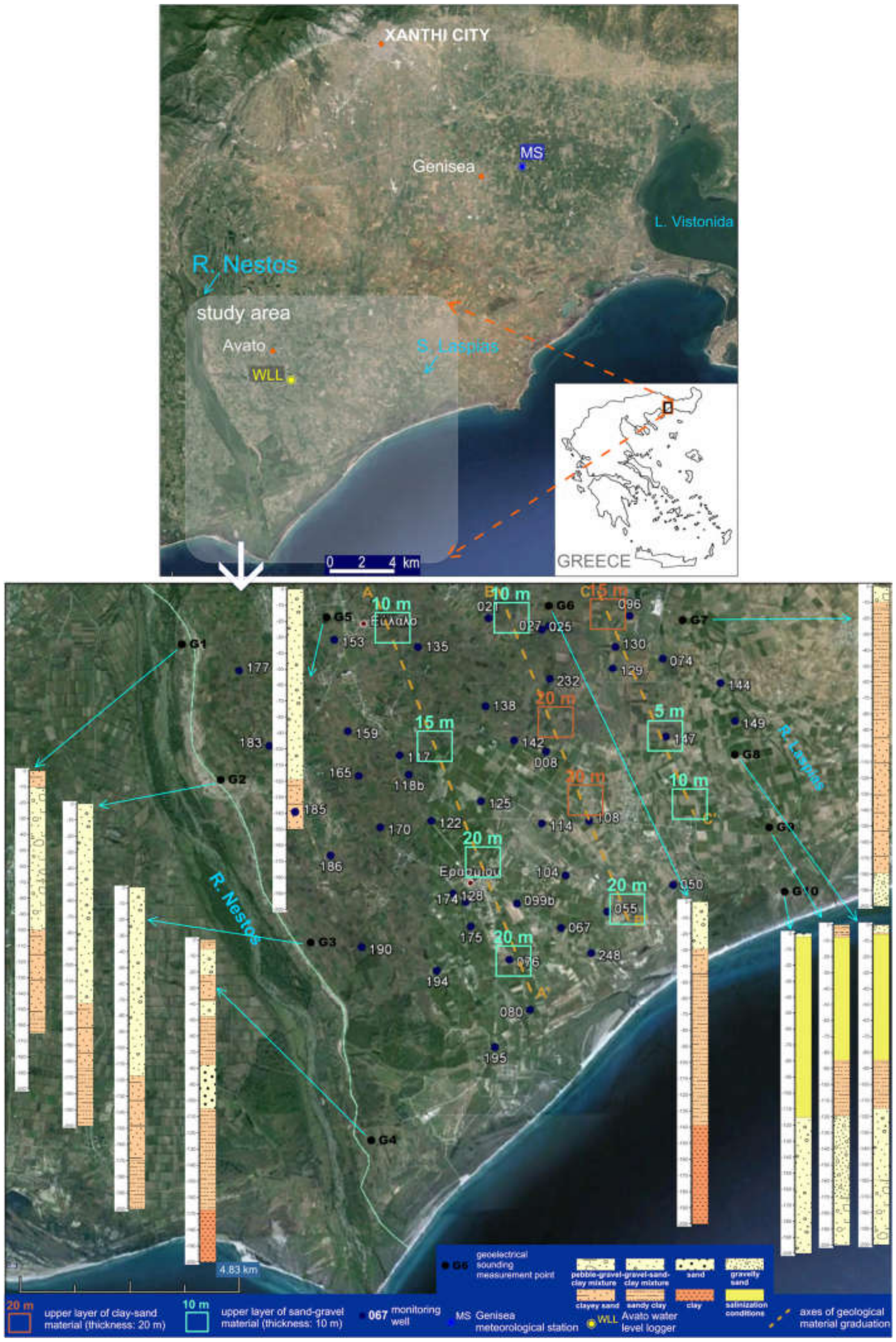

Figure 1. Overall presentation of conducted field activities in the study area (WLL: water level logger, MS: meteorological station) (basemap source: Google Earth Image 2020).

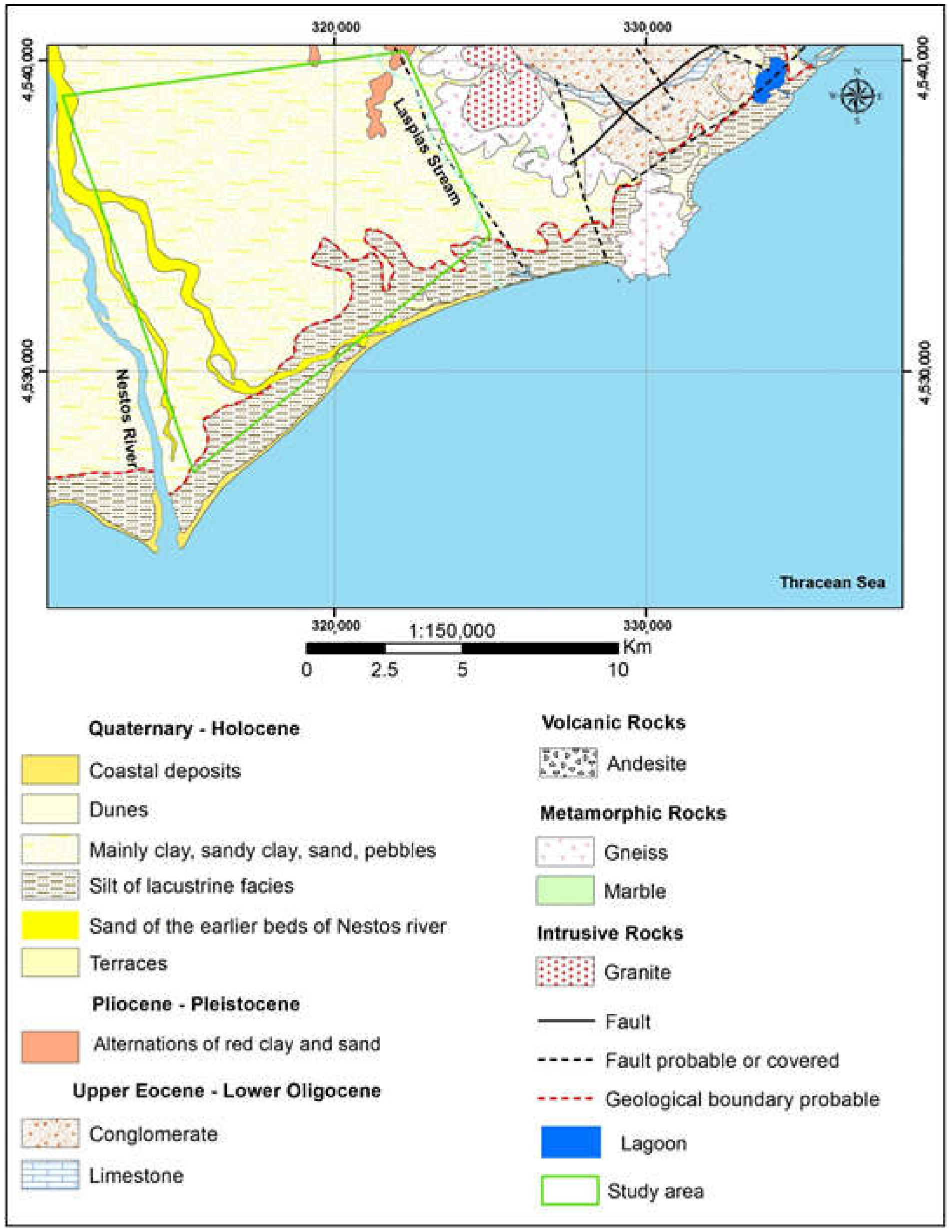

Figure 2. Geological map of the research area (source geological map of Greece IGME 1980; [49]).

3. Geological Setting

The research area is situated in Holocene delta environment deposits with a thickness of some tens of meters built by River Nestos and sub-streams. These deposits consist of alternate clay, sand and silt layering, have resulted in a broad range of formational and depositional tasks, that produced a very diverse geological domain. In addition, due to delta marshes the existence of organic clay at some spot is identified. The advancement of the eastern Nestos delta in conjunction with flooding conditions has been contributory in shaping low potential aquifers in the research area.

Recent as well as previous [46] field investigations were conducted (i.e., installation of monitoring wells, geophysical measurements, borehole loggings) in order to analyze the geological setting of the study area. The aforementioned studies showed that within the northern part of the research area, alternate clay—sand layering expands downwards down to a depth of approximately 30 m. Next, a marly layer of about 50 m thickness exists, while at a depth lower than 80 m, similar clay—sand layers are also present [46].

The covered area of east delta plain is approximately 176.4 km^2, and only 60% or about 106.63 km^2 are cultivated. In addition, the coastal saline zone includes uncultivated regions with a total coverage of about 45 km^2. Taking into account the respective hydrological figures of Nestos Delta flatland (infiltration approximately 15% and mean yearly rainfall from 1965 to 1996: 546.9 mm), the annual infiltration was evaluated at about 10.8×10^6 m^3 for the potential cultivated area of 131.4 km^2 (176.4 − 45.0 = 131.4). The total irrigated area expands up to 89.89 km^2, and the 35.0 km^2 of which cover the watering needs from the nearby River Nestos. The remaining areas cover watering necessities by pumping groundwater. Bearing in mind the variety and the proportions of the cultivations in the study area, the yearly water utilization was reckoned at about 27×10^6 m^3. Considering the values of the above fundamental factors of groundwater hydrologic equilibrium (infiltration and water utilization), a shortage of approximate 16×10^6 m^3 water was estimated [46]. A minor part of this deficiency is restored by Nestos riverbed infiltration, and the rates rely partly on the length of the old smaller and buried riverbeds and partly on the distance from the actual active riverbed.

In the research area ten (10) geoelectrical soundings were conducted, with the main target being to identify the stratigraphy of the region (Figure 1). This task was executed as stated by the Schlumberger method for measuring soil resistivity. The maximum electrodes spread was 800 m (AB/2 = 400 m) for G1 and G5 cases and 1000 m (AB/2 = 500 m) for all the others. The survey spots were determined so that they can cover parts of the research area where the stratigraphy was not well identified. Thus, the survey spots are situated across River Nestos (3 surveys), across stream Laspias (3 surveys) and finally across the northern border of the research area, about 9.5 km from the seashore (4 surveys).

The results of the geoelectrical soundings correlate directly with stratigraphy data. The G1 survey was the only case in which a clay-sand layer remained undetected by the sounding. It is worth mentioning that any interpretation of a geoelectrical sounding must take into account surface geology data as well as borehole intersections.

High conductivity values during the geophysical investigations within that part of the study area, are attributed to percolation of saline surface water that is originated from Laspias stream (as described in more details §6). The results of the G9 and G10 surveys are in cohesion with all the other researches and surveys in this region. The G9 and G10 spots are situated next to the seashore, where the respective indicators and quality specifications of the groundwater have the worse values due to the intrusion of seawater. The G8 survey (located 5 km away from the seashore), came up with saline groundwater state, a somehow unexpected outcome. This finding should be examined further because there might be a potent affiliation with the geothermal field of the broader region that exists deeper below.

The outcome of all ten (10) surveys—electrical soundings (Figure 1) resulted in 6 explicit dominant geoelectrical formations classified in proportion to the values of the specific electrical resistivity [50,51]: (i) a mixture of pebble-gravel (50–220 Ohm·m), (ii) gravel (25–50 Ohm·m), (iii) sand (20–25 Ohm·m), (iv) clayey sand (16–20 Ohm·m), (v) sandy clay (11–16 Ohm·m), (vi) clay (8–11 Ohm·m) and salinization conditions (<8 Ohm·m). The prevalence of clay together with clay-sand materials in every part of the research site is very clear.

Finally, it must be mentioned that the presented resistivity values can only be validated in this research region, and so the span of hereby values is smaller, in contrast with the value range depicted in relevant international bibliography, for the geological formations of the research area.

4. Hydrometeorological Conditions

In Figures 3–5, hydrometeorological data are presented, for the period 1966 to 2013. Figure 6 shows the average monthly rainfall for the periods 1966—2012, 1985—2012, 1995—2012, 2000—2012.

After analysis and processing of all the above diagrams of the preceding figures, the following outcomes obtained [52]:

- ✓ A peak value of precipitation is observed in November and December 1996 (the big rainfall event and the devastating floods of 30 November and 1 December, 1996).
- ✓ Characteristic is, for the season, the high precipitation value for the summer months of July and August 2002 and 2005, as well as the very high precipitation values of December 2003 and October 2010.
- ✓ Significantly higher mean monthly precipitation, is presented, for October periods of 2000—2012 and 1995—2012, while characteristic is the average monthly precipitation value for November period 2000—2012, which is clearly less than the periods 1966—2012, 1985—2012 and 1995—2012, a thing that is not identified for all other months for the period 2000—2012.

These outcomes are valuable considerations for the evaluation of natural groundwater recharge fluctuations of the research area, where alluvial aquifers are being formed.

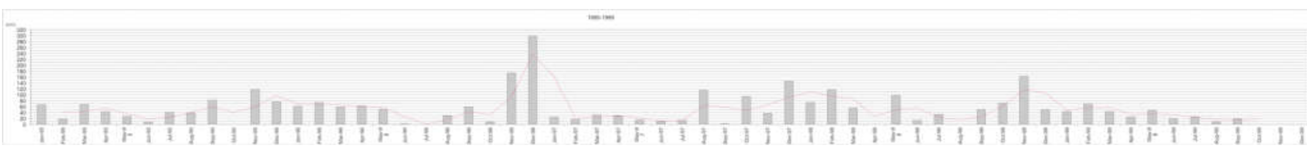

Figure 3. Monthly rainfall (meteorological station of agricultural research in Genisea Xanthi) and moving average for the period 1995 to 1999.

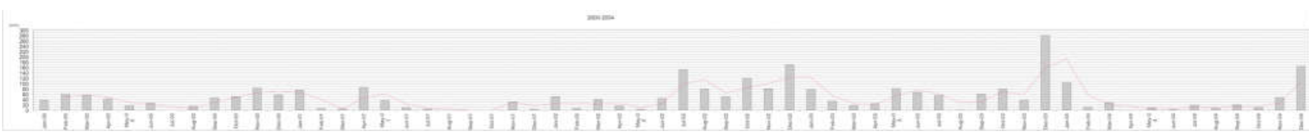

Figure 4. Monthly rainfall (meteorological station of agricultural research in Genisea Xanthi and rainfall station of the Section of Hydraulic Engineering, Department of Civil Engineering) and moving average for the period 2000—2004.

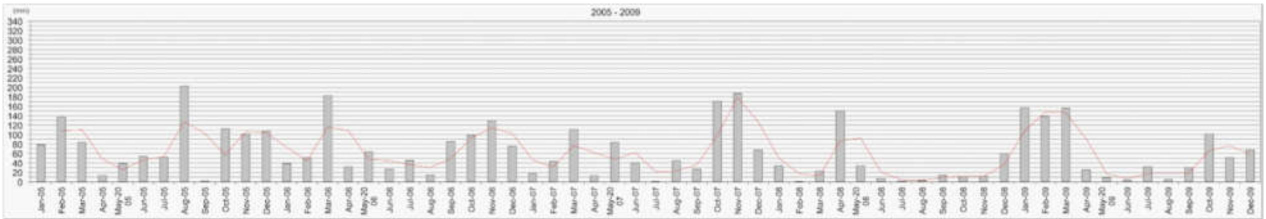

(**a**)

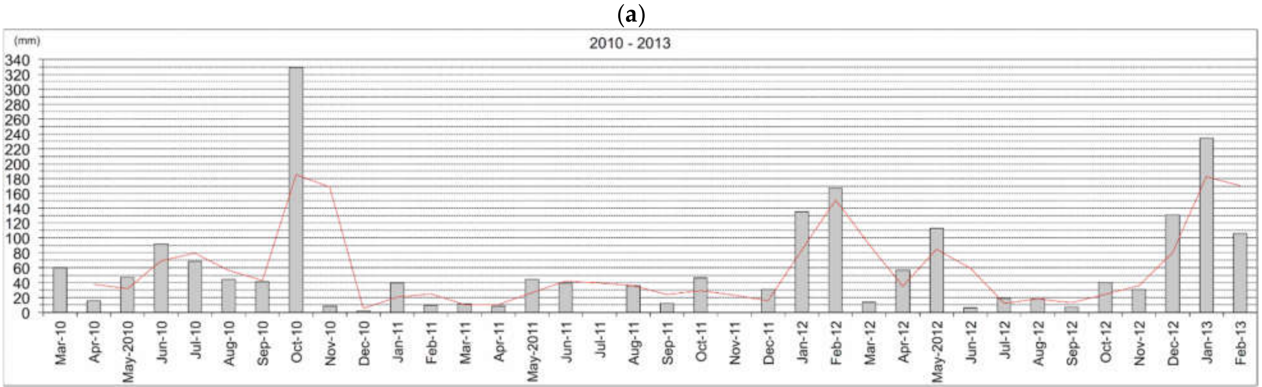

(**b**)

Figure 5. Monthly rainfall (rainfall station of the Section of Hydraulic Engineering, Department of Civil Engineering, Democritus University of Thrace, Xanthi and meteorological station of the National Observatory of Athens—Institute of Environmental Research) and moving average for the period (**a**) 2005—2009 and (**b**) 2010—2013.

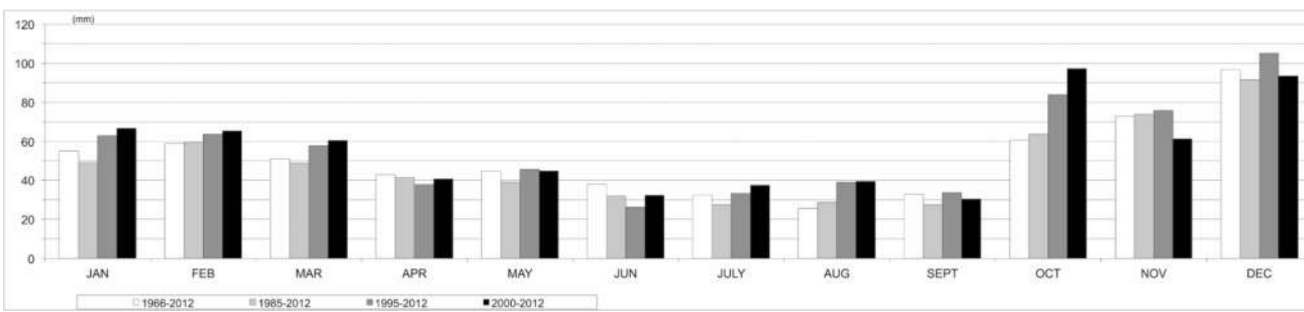

Figure 6. Average monthly rainfall for the periods 1966—2012, 1985—2012, 1995—2012, 2000—2012.

5. Hydrogeological Setting

The area is located outside the zone with a large proportion of permeable material (Nestos paleogeographic axis) and therefore, the materials hosted expected to have small particle diameter (sands and clays).

Two hydrogeological systems are identified in the research area, which are situated within the quaternary coastal and alluvial deposits of the broader region [46]. The first hydrogeological system is a shallow one, and it consisted by of phreatic to semi-confined aquifers with a thickness of approximately 30 m. The main recharge of this hydrogeological system is mainly from precipitation and partly from nearby small streams and canals. The second deeper hydrogeological system of the study area, incorporates alternate confined aquifers with a thickness of approximately 200 m. Recharge of the second system derives partly from river Nestos infiltration through old buried river beds, and partly from lateral groundwater inflows originate from the neighboring hydrogeological basin of Vistonida lagoon.

Estimation of the groundwater hydraulic parameters of the research area aquifers after analyzing the pumping test data from 11 selected wells in the broader research area derived in values for [46]: (1) transmissivity (T), ranging from 4.0×10^{-4} to 1.1×10^{-2} m^2/s, (2) storage coefficient (S), ranging from very low values to 10^{-3}, rendering the aquifers of the research area as mainly confined westward, and in several sites as semi-confined. The major groundwater flow direction (Figures 7 and 8) is from northwest towards south with a little flow from northeast and central parts of the research area towards south.

The first aquifer system is recharged mainly by rainfall and slightly by percolation from the upstream hills aquifers. The shallow aquifer system in the region over the past decade, was exploited by a large number of shallow wells (up to 1000) with small diameter, up to a depth of 15 m. Nowadays, few of them are remaining operational and they have been replaced by deeper wells up to 50 m depth. At the eastern part of the study area, the limited groundwater potential, the drainage constructions, as well as the particular geological structure have conducted to the groundwater and soil salinization in the region. When the area receives large amounts of precipitation, the effect of increasing of the shallow aquifer systems discharge is occurred, also taken into account that the infiltration rate for the region is over 15%.

The second aquifer system (deep aquifer) is recharged to a great extent by groundwater percolation inflows through the Nestos paleogeographic axes (buried old stream beds), and partly by lateral groundwater inflows coming from the adjoining Lake Vistonida hydrogeological basin. This deeper aquifer system is being exploited by deep wells (about 50) the depth of which reaches 200 m.

In this study, the groundwater level fluctuations were monitored in the study area during the period 2007—2009 and in 2013 and piezometric maps of groundwater system of the study area were compiled for the upper phreatic aquifer system and the underlying deeper pressurized aquifer system of the study area, such as charts of groundwater level fluctuations. Based on the interpretation of these diagrams and maps (Figures 7 and 8 show the piezometric maps of the phreatic aquifer for the wet and dry periods of 2014) the following general conclusions were drawn:

- ✓ The main groundwater recharge source of the upper unconfined aquifer system occurs mainly from N–NW part of the study area from the River Nestos and old riverbeds, as well as from the local irrigation network and the northeastern part of the Laspias stream (dashed polylines in Figures 7 and 8).

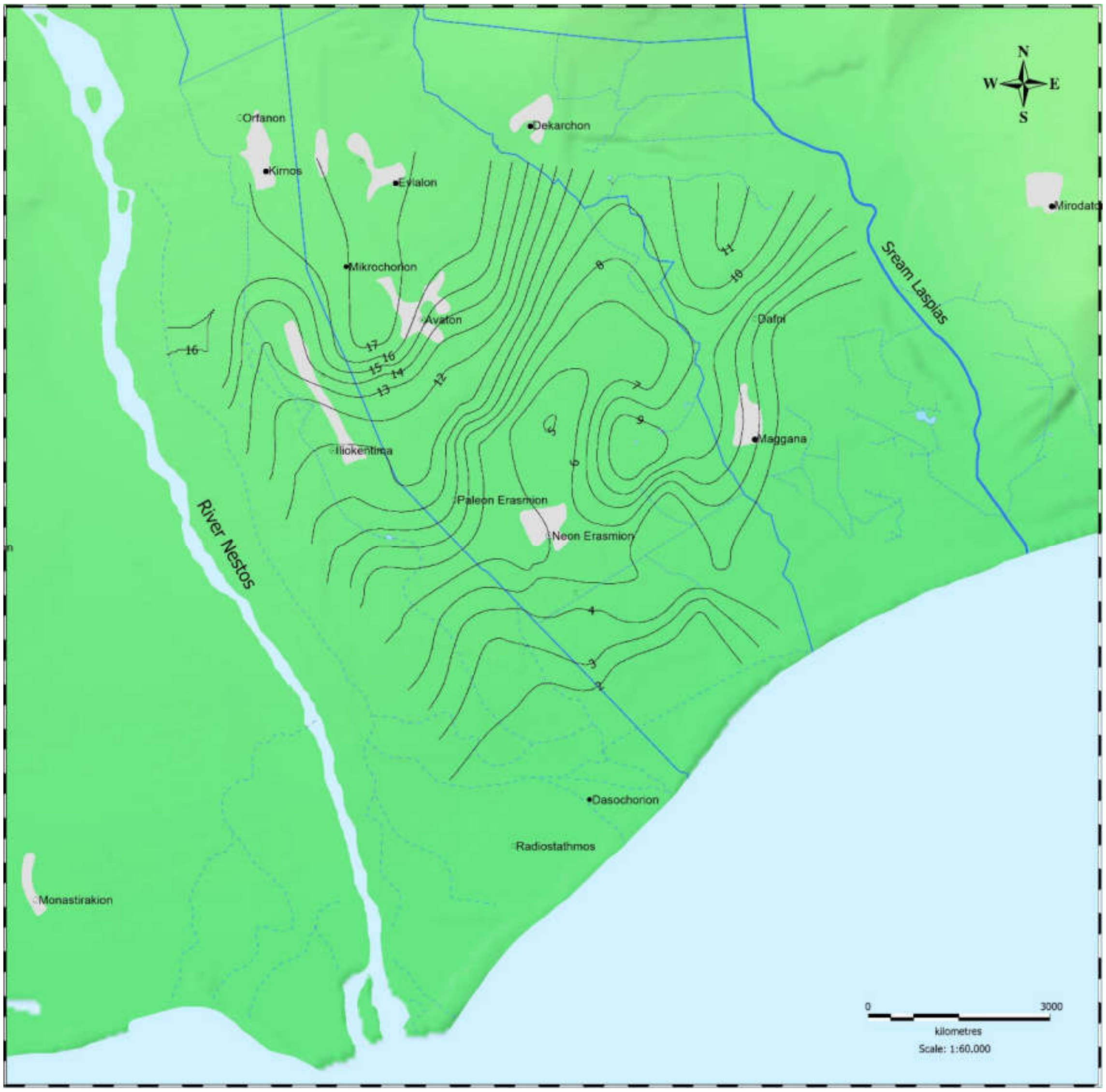

Figure 7. Piezometric map of the unconfined aquifer system at April 2014.

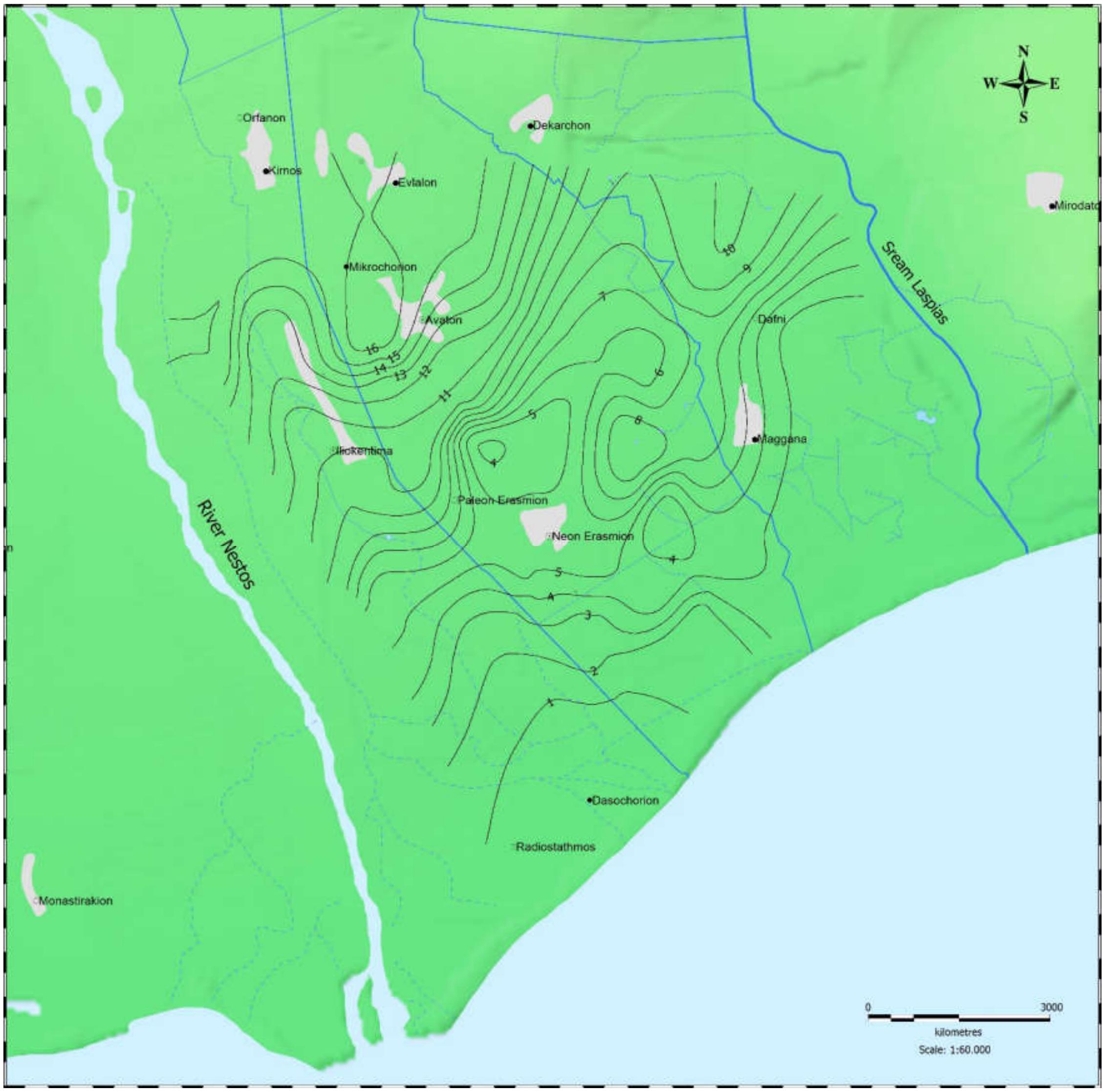

Figure 8. Piezometric map of the unconfined aquifer system at October 2014.

6. Hydrochemical Setting

The groundwater samples from the research area were collected in polyethylene bottles following the procedure described by Rainwater and Thatcher [53]. The chemical analyzes were performed within 24 h, from the moment of sampling, in the Laboratory of Technical Geology of the Department of Civil Engineering of the Democritus University of Thrace. The measurements of cations and anions (with the exception of that of chlorine ions) were carried out using a spectrophotometer. The determination of chlorine ions (Cl^-) was performed by the titration method, as described in detail in the relevant manual of the American Public Health Association [54], with the gradual addition of 0.1 N $AgNO_3$. All determinations concerning measurements of specific electrical conductivity values (μS/cm), temperature (°C) and active acidity (pH), were performed in the field using portable instruments. Sodium (Na^+) and potassium (K^+) ions were determined using a flame photometer. In addition, during the pumping period July-August 2009, 30 samples were taken for the determination of deuterium (δD ‰) and oxygen-18 (δO-18 ‰) isotopes. The samples were taken in 100 mL polyethylene vials and packed in a suitable device—transfer refrigerator. These determinations were carried out by the Institute of Applied Geosciences of the Technische Universität Darmstadt, Germany.

To monitor the groundwater quality of the survey area, a network of appropriate 30 sampling wells was selected, in such a way in order to correspond to the under-investigation aquifer and to cover the area as well as possible. The research periods basically include the pumping periods (July–August) of the years 2006, 2007, 2008, 2009, 2013 and 2014 where chemical analyzes were carried out.

Two representative periods (8/7/2009 and 04/07/2013) of the investigated aquifer were selected for presentation within the framework of the present manuscript. The examined parameters were: Ca^{2+}, Mg^{2+}, Na^+, K^+, HCO_3^-, Cl^-, SO_4^{2-}, NO_3^-, NO_2^-, NH_4^+, PO_4^{3-}, SiO_2, Fe^{2+}, Mn^{2+}, alkalinity P, alkalinity M, hardness (permanent, non-permanent, total), pH, electrical conductivity (EC).

In Figure 9, the spatial distributions of chlorides is presented for the study area, where it is observed that the upper unconfined aquifer layer is salinized within the eastern and south-eastern boundaries of the area.

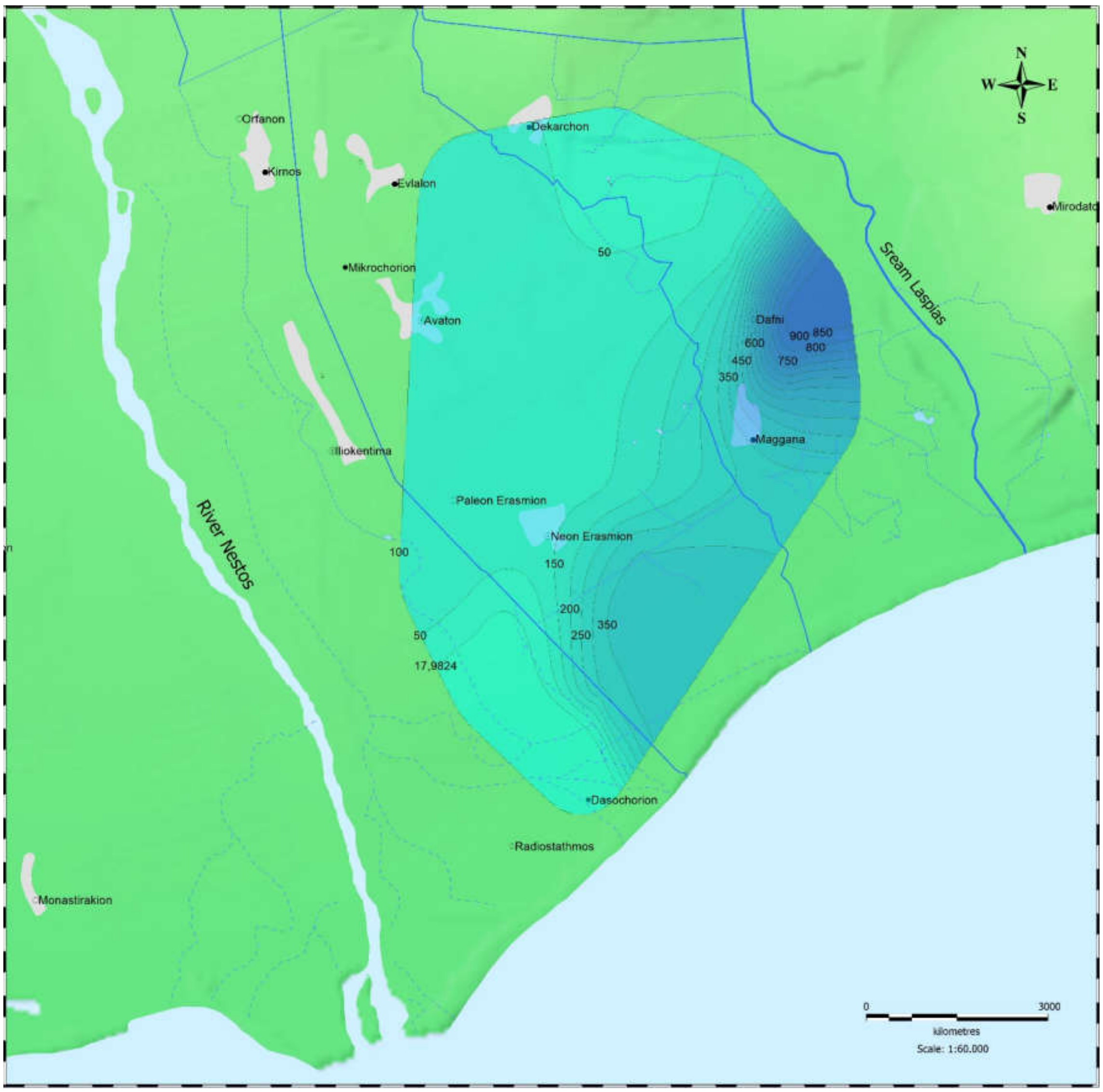

Figure 9. Chloride ion distribution map (Cl^-) of the unconfined aquifer of the research area—2014.

In Table 1 statistical analysis of some of the major chemical constituents from groundwater samples during the irrigation periods (July) 2009 and 2013 is presented (maximum drinking water levels are mentioned, Ca^{2+}: >100 mg/L, Mg^{2+}: >50 mg/L, SO_4^{2-}: >250 mg/L,

HCO_3^-: >500 mg/L, PO_4^{2-}: >0.50 mg/L, NO_3^-: >50 mg/L, NO_2^-: >0.5 mg/L, NH_4: >0.5 mg/L, Cl^-: >250 mg/L, K^+: >12 mg/L, Na^+: >200 mg/L, Fe^{2+}: >0.25 mg/L, Mn^{2+}: >0.10 mg/L, EC: >2500 μS/cm [51]).

The values of specific electrical conductivity EC of the samples ranging from 417 to 5100 μS/cm for 2009 and from 311 to 3750 μS/cm for 2013 (Table 1). The higher values (>4000 μS/cm) are observed in SE part of the study area, while the majority of the wells presents specific electrical conductivity of around 1000 μS/cm. For the wells where low values of specific electrical conductivity are observed, are these which are parallel to the irrigation canal and recharged directly with good water quality from the river Nestos.

Table 1. Statistical analysis of some of the major chemical constituents from groundwater samples during the irrigation periods (July), 2009 and 2013.

	Ca^{2+} (mg/L)	Mg^{2+} (mg/L)	SO_4^{2-} (mg/L)	HCO_3^- (mg/L)	PO_4^{2-} (mg/L)	NO_3^- (mg/L)	Cl^- (mg/L)	EC (μS/cm)	pH	Temp. (°C)	K^+ (mg/L)	Na^+ (mg/L)	Fe^{2+} (mg/L)	Mn^{2+} (mg/L)
							2009							
min	59.66	26.24	50.00	162.26	0.12	0.00	15.60	417.00	6.72	16.10	11.00	19.00	0.01	0.40
max	875.07	369.85	1112.50	800.32	8.77	60.00	1320.20	5100.00	7.57	22.10	200.00	880.00	1.99	2.90
aver	197.90	93.25	245.88	384.25	1.34	14.25	322.75	1868.92	7.01	18.11	94.33	246.58	0.81	1.21
SD	215.58	90.72	285.06	176.49	2.40	18.25	407.10	1478.12	0.23	1.67	73.07	254.81	0.67	0.65
							2013							
min	34.35	7.78	16.40	134.20	0.21	0.00	1.77	311.00	7.10	16.20	1.60	9.00	0.00	0.00
max	488.16	77.76	465.00	762.50	10.30	120.00	813.81	3750.00	7.76	19.50	54.00	530.00	2.89	2.70
aver	254.02	36.05	190.45	392.03	1.90	31.83	247.42	1763.42	7.33	17.76	12.97	187.92	0.56	1.04
SD	141.40	20.60	157.98	190.14	2.86	43.96	266.58	1134.67	0.18	1.08	14.16	187.26	0.83	1.02

The concentration values of Cl^- ranging from 15.6 mg/L to 1320.2 mg/L for 2009 and from 1.8 mg/L to 819.8 mg/L in 2013 with around 30% of the values of water samples clustered close to the mean value (216.64 mg/L) or above it. Values less than 25 mg/L are apparent in the western part of the study area. Large concentrations of Cl^- (>200 mg/L, higher than acceptable limit) make the local water undrinkable.

The concentrations of nitrate (NO_3), are ranging from 0 mg/L to 60 mg/L for 2009 and from 0 mg/L to 120 mg/L for 2013, with three (3) of the thirty (30) boreholes to be out of the acceptable limits (allowable: 50 mg/L), while the concentrations of nitrite (NO_2), ranging from 0.013 mg/L to 0.358 mg/L, with five (5) of the thirty (30) wells out of the acceptable limits (permissible limit: 0.1 mg/L).

Regarding the suitability of the water samples analyzed for irrigation, based on TDS (total dissolved solids), SAR (sodium adsorption ratio), the concentrations of sodium (Na), chlorine (Cl^-), bicarbonate ion (HCO_3^-), the value criteria %E.sp (%Na, alkalinizing degree) and conductivity EC for 2009 and 2013 and evaluating the results according to ratings-rankings by Ayers [55], Richards [56] and Wilcox [57], generally all samples identified as problematic.

It is recognized that:

- The majority of water samples classified into classification classes in which there is a high or very high salinity. This shows the seriousness of the problem of seawater intrusion into the groundwater aquifers of the area and thus makes it necessary to take measures to control salinity and crop only salinity resistant plants.
- The largest proportion of the samples, the effect of salinity on fruiting classed with growing problems class, and there are also samples taken from specific wells in which the effect of salinity on fruiting classified as serious problems. It is obvious that the effect of salinity on groundwater, and consequently on irrigation is higher in areas closer to the sea. This fact is in direct consequence with the emerge of various problems in agriculture, land degradation and thus gradually reduction of agricultural yield.

- According to the criterion of Wilcox water quality, 14 wells classified as 'good', 5 wells as 'accepted', 3 wells as 'doubtful' and 7 wells as 'excellent'. In part of the study area recharged by the river Nestos and the irrigation canal, waters are characterized from 'excellent' to 'good', while in the rest of the region are characterized from 'acceptable' to 'doubtful'.

In research area, the TDS (total dissolved solids) ranging from 267.3 mg/L to 3.269.1 mg/L in 2009 and from 199.3 mg/L to 2403.7 mg/L for 2013. Rates TDS > 3000 mg/L were measured in the water of just a well. Regarding the suitability of the analyzed groundwater sample for drinking from domestic animals the overall amount of the samples are characterized as appropriate for 'watering' all domesticated animals.

To avoid erroneous diagnosis of seawater intrusion due to a temporary increase in TDS, Revelle [58] proposed as a criterion of seawater penetration, the use of the ratio $Cl/(CO_3 + HCO_3)$ in meq/L, which is also known as Revelle coefficient (R). Values of Revelle (R), which fluctuate from 1 to 10, indicates slight to moderate pollution from seawater intrusion, while values greater than 10 may be regarded as evidence of a serious pollution of seawater intrusion [51]. Based on Revelle values (R), it is concluded that the water of the studied area is characterized from 'good' to 'slightly contaminated' by seawater intrusion and 'serious polluted' in some places of the SW part.

From the analysis of Piper and Durov charts (Figures 10 and 11) as well as the correlation plot of $SO_4 + HCO_3$ vs. Cl (Figure 12), obtained from 30 sample wells, it is concluded that the majority of the samples are in the range of conservative mixture between freshwater and saltwater, and some of the samples show significant salinity problems due to possible seawater intrusion.

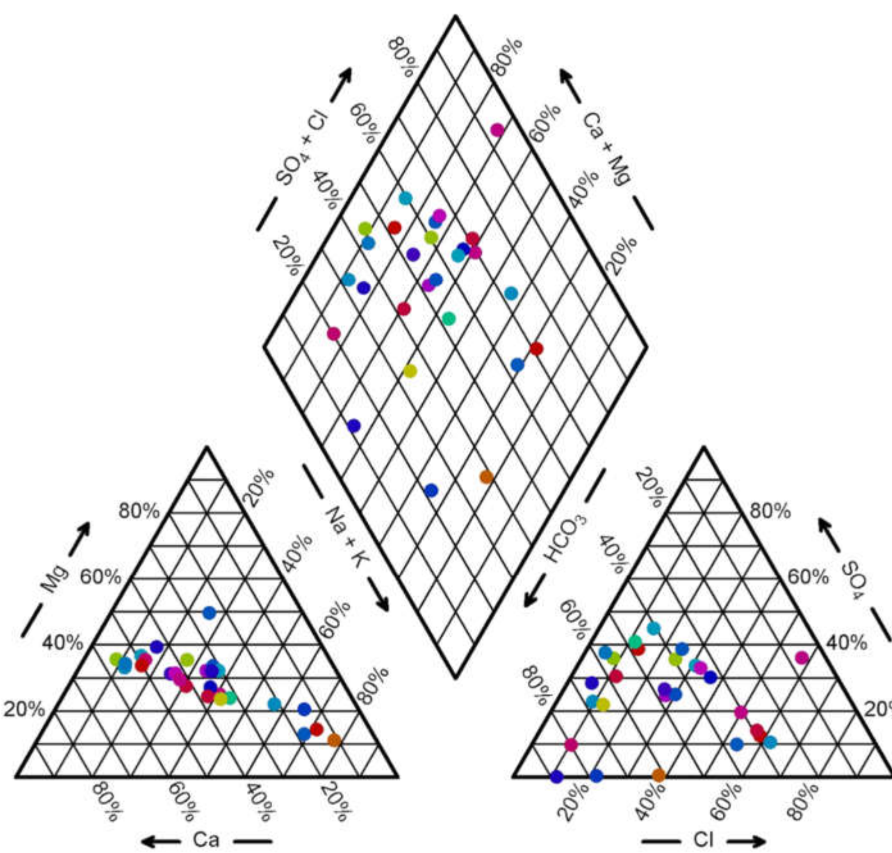

Figure 10. Trilinear Piper diagram for all the wells of the research area (2014).

Based on SAR, TDS, EC values and concentrations of Na^{+}, Cl^{-} and HCO_3^{-} of water samples in 2009 and 2013, the restriction level on use was estimated (DRU, degree of restriction on use) [59,60], and characterized [52,61]:

1. Regarding salinity (affecting water for plant growth), as small to medium (SM) in the majority of samples, and as severe (S) in a few of them (4),
2. Regarding the permeability (affecting the rate of water infiltration in soil), as minimal (N), small and average (SM),
3. Regarding the specific ion toxicity (affecting sensitive plants), as minimal (N) to severe (S), with typical the surface irrigation where several samples of groundwater assessed as small to average degree (SM) in restriction on use (DRU).

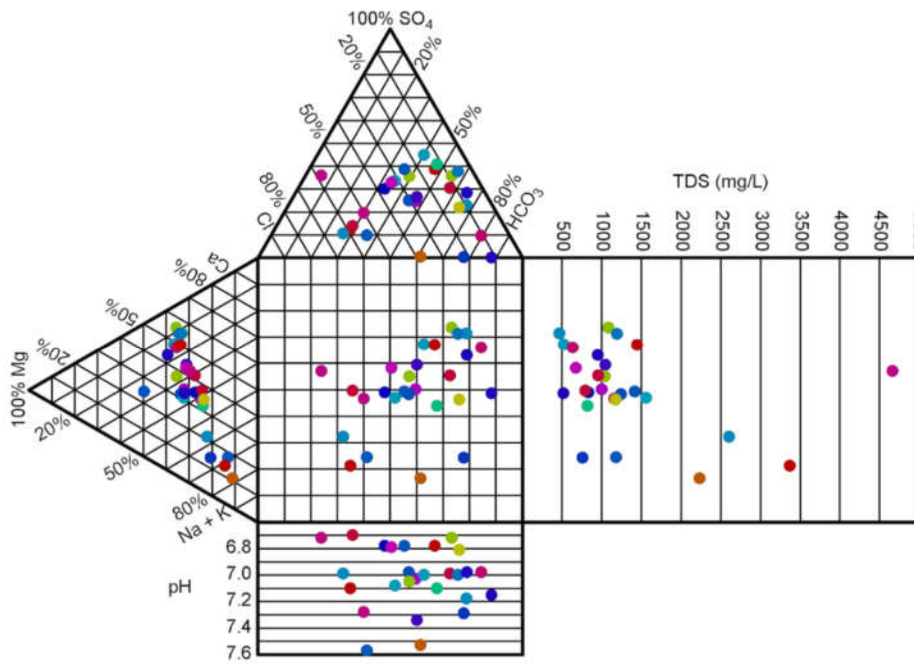

Figure 11. Durov diagram for all the wells of the research area (2014).

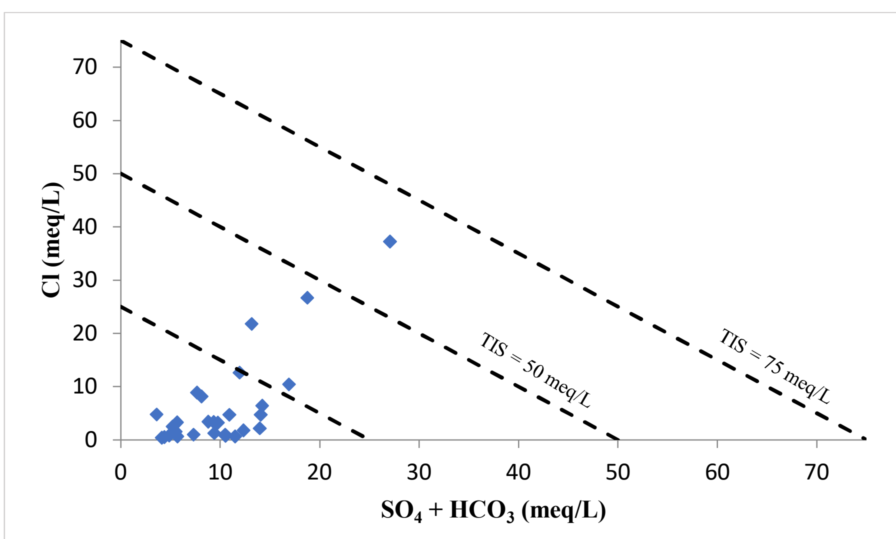

Figure 12. Correlation plot of SO_4 + HCO_3 vs. Cl diagram for all the wells of the research area, also showing isolines of total ionic salinity (TIS) lines for reference (2014).

7. Stable Isotopic Signatures of Groundwaters

The results for the isotope analysis reveal that the groundwater from of the study area is isotopically heavy. This can be seen from the plot of δD as a function of $\delta^{18}O$ (Figure 13), where most points fall close to the global meteoric water line (GMWL: $\delta^2H = 8\delta^{18}O + 10$) with heavier isotopic values. The plot shows a pattern of two clusters of points; one very close to GMWL and the other away from it. The former represents isotope results for the wells located to the east of the study area close to the Aegean Sea. This implies that the aquifer in the part of the study area is subjected to recharge mainly from the sea by seawater intrusion. Ideally, oceanic water or seawater would fall below the meteoric water line but the observed result is due to dilution during mixing with freshwater in the aquifer. Deviation from the meteoric water line further left indicates the part of the recharge that originates from the freshwater of the Nestos River.

Considering the local meteoric water line for the Mediterranean region which the Mediterranean meteoric water line (MMWL: $\delta^2H = 8\delta^{18}O + 22$), all the groundwater samples fall below the MMWL meaning that the groundwater aquifer contains isotopically heavy water which can be attributed to seawater intrusion resulting from continued over pumping.

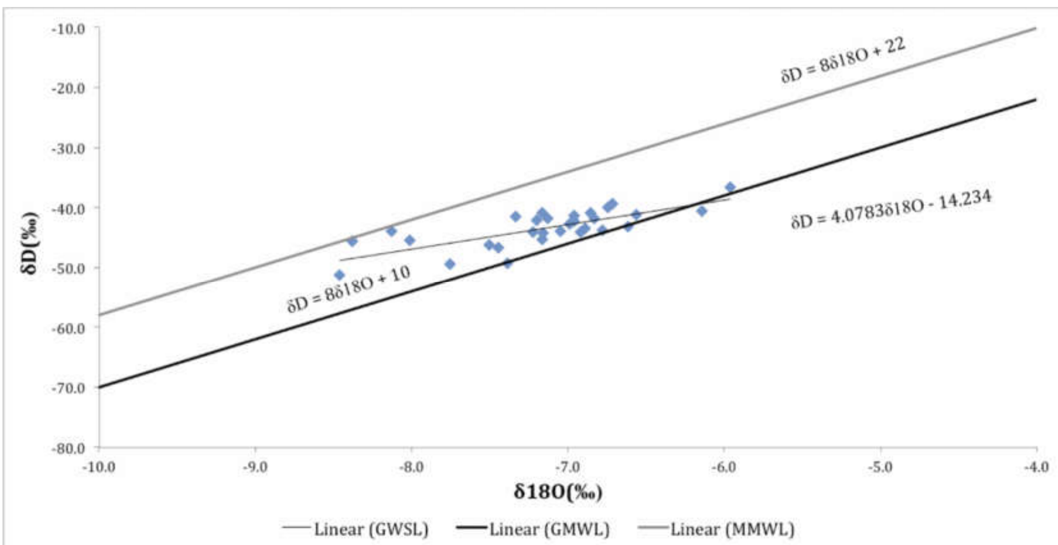

Figure 13. Plot of $\delta D(\delta^2H)$ and $\delta^{18}O$ values for groundwater samples stable isotope results.

8. Mathematical Modelling

8.1. Description of the Numerical Code (Finite Difference Method)

The groundwater flow of the studied aquifer system was simulated by using the finite difference method, after the application of the USGS MODFLOW-2005 code. MODFLOW-2005 [62] simulates steady and non-steady flow in an irregularly shaped flow system in which aquifer layers can be confined, unconfined, or a combination of confined and unconfined (Figure 14).

The three-dimensional movement of ground water of constant density through porous media is expressed by the partial-differential equation [63] as follows:

$$\frac{\partial}{\partial x}\left(K_{xx}\frac{\partial h}{\partial x}\right)+\frac{\partial}{\partial y}\left(K_{yy}\frac{\partial h}{\partial y}\right)+\frac{\partial}{\partial z}\left(K_{zz}\frac{\partial h}{\partial z}\right)+W=S_s\frac{\partial h}{\partial t}$$

where:

→ K_{xx}, K_{yy}, and K_{zz} are values of hydraulic conductivity along the x, y, and z coordinate axes, which are assumed to be parallel to the major axes of hydraulic conductivity (L/T);

→ h is the potentiometric head (L);
→ W is a volumetric flux per unit volume representing sources and/or sinks of water, with W < 0.0 for flow out of the ground-water system, and W > 0.0 for flow into the system (T^{-1});
→ SS is the specific storage of the porous material (L^{-1});
→ t is time (T).

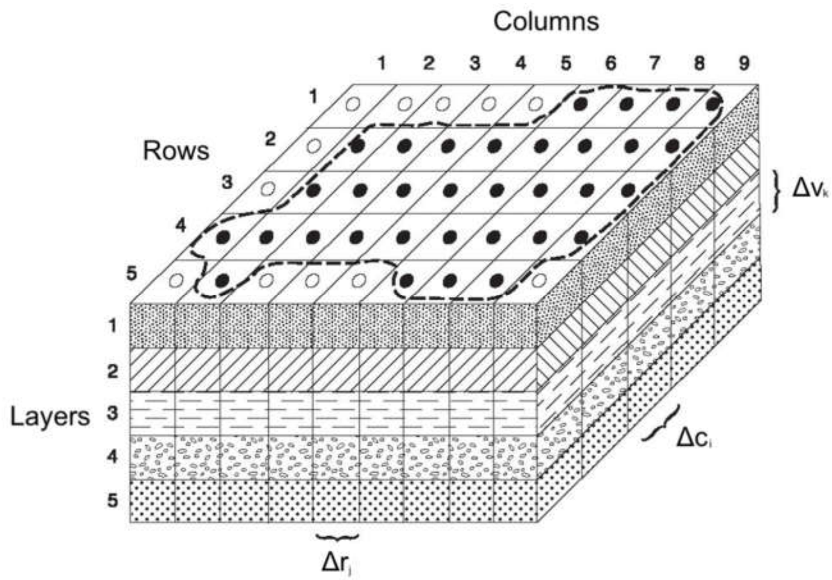

Figure 14. A discretized hypothetical aquifer system [64].

8.2. Spatial Discretization

The developed groundwater flow model expands in an area of 140 km² with the aquifer being represented by a 30 m thick layer (Figure 15), that simulates an unconfined aquifer and the grid used is 200 × 200 m. The model run under transient conditions -except for the first stress period which is used as a reference period. The surface elevation used in the model corresponds to a 30 × 30 m digital elevation model (DEM) taken by NASA (ASTER GDEM 2).

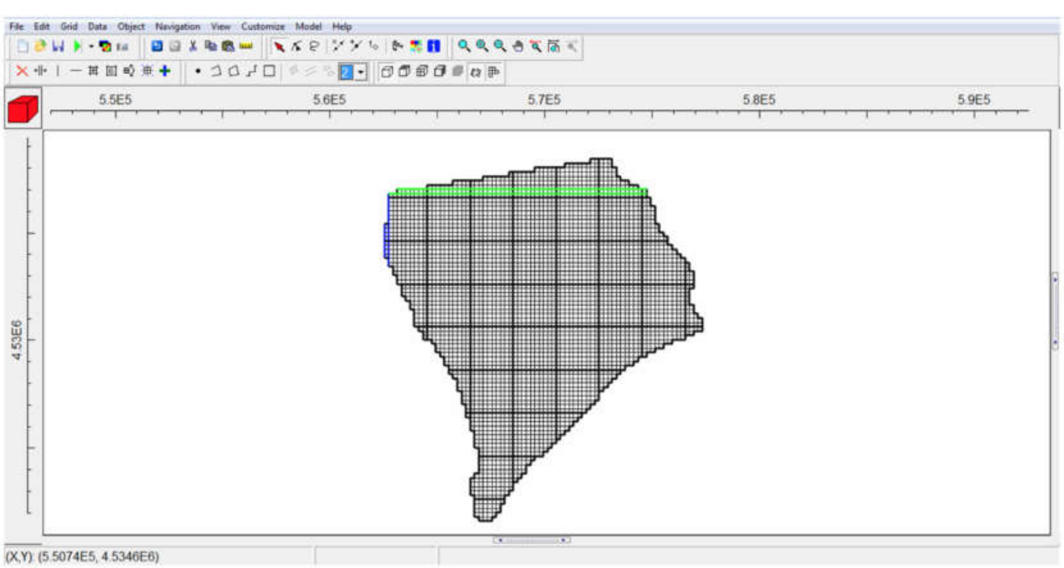

Figure 15. Model grid and graphical user interface of ModelMuse.

8.3. Boundary Conditions

The boundary conditions are used to establish the hydrological processes taking place in the investigated aquifer (Figure 16). In this study, the MODFLOW-2005 packages used to represent the boundary conditions are:

- General head boundary (GHB): This package is used to introduce the general groundwater flow conditions in the area. The hydraulic head used is 16 m.a.s.l. and is introduced in the northern boundary of the model area. The selected head is based on the piezometric maps mentioned before (Figures 7 and 8). The hydraulic conductance used in the simulation is 5 m^2/d.
- River (RIV): In the western part of the study area the Nestos river is simulated using the river package. The river depth for the in the reference period is 1.57 m., while the hydraulic conductance in the beginning of the simulation is 30 m^2/d.
- Drain (DRN): The drain package is used to simulate the Laspias stream in the eastern part of the model with a hydraulic conductance of 10 m^2/d.
- Time variant specified head (CHD): This package is used for simulating the discharge of the model to the sea. As such, the hydraulic head used throughout the simulation is 0 m.a.s.l.
- Head observation (HOB): This package is used for introducing the hydraulic head observations from the field surveys, which are later used for the calibration of the model.
- Recharge (RCH): This package is used across the model to implement the inflow from precipitation. The infiltration coefficient used is 15% of the precipitation in the reference period (which had 18 mm of precipitation).
- Well (WEL): The package is used for introducing the pumping for irrigation in the study area. The number of pumping wells in the area is very large (>2000), so for optimal data management the pumping was distributed across the model area (Figure 17). The irrigation period is from June to August.

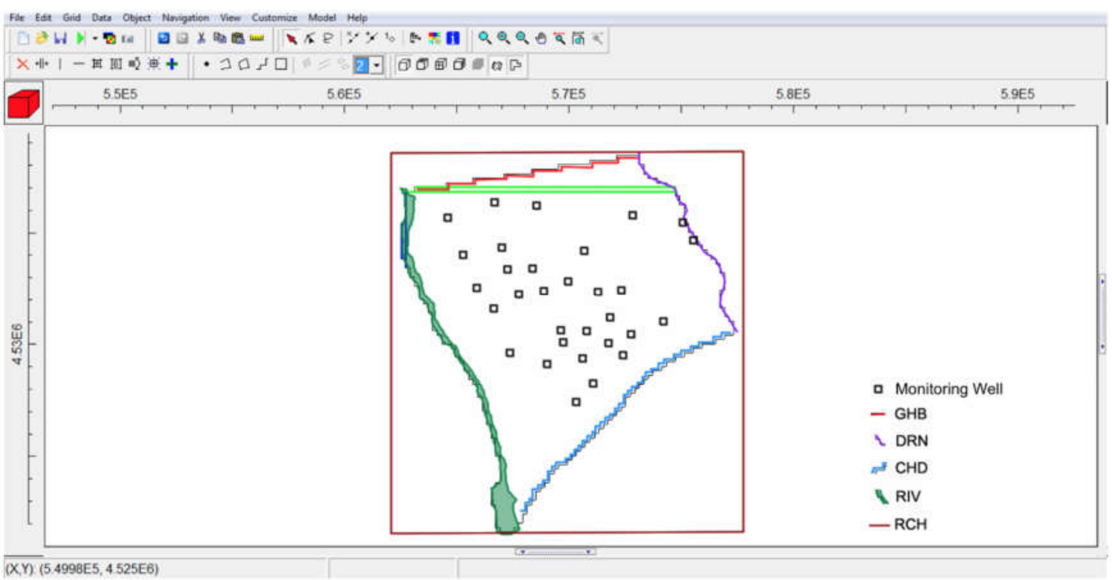

Figure 16. Model boundary conditions and used MODFLOW packages.

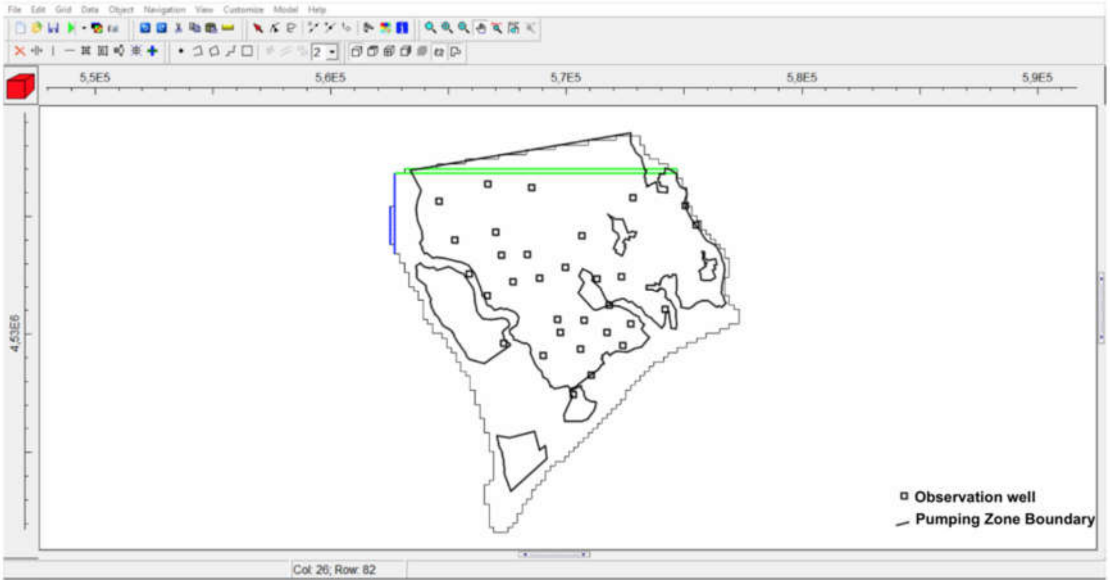

Figure 17. Monitoring wells network and pumping zones of the mathematical model.

8.4. Hydraulic Parameters of the Model

The hydraulic parameters values are based on the pumping test analyses from various locations within the study area. The evaluation gave a range between 0.78 and 15.22 m/day, with an average value of 7.92 m/day. The same set of pumping tests is used for estimating the storativity coefficient, with extracted values varying between 1×10^{-3} and 2.8×10^{-2} with a mean value of 6.79×10^{-3}.

8.5. Time Discretization

The time discretization of the model is based on the hydrogeological conditions that were defined during the field survey. The model has 13 stress periods (each corresponding to a calendar month) with daily time steps in each period, with the first one having steady state flow conditions and the rest transient (Table 2). Pumping was implemented in stress periods 6, 7 and 8, which correspond to June, July and August respectively. The observations used in the model are assigned in the end of the 4th and 10th stress periods.

Table 2. Time discretization and flow conditions of the groundwater flow model.

Stress Period	Time Step	Calendar Period	Flow Conditions
1	1	31/1/2007	Steady state
2	28	2/2007	Transient state
3	31	3/2007	Transient state
4	30	4/2007	Transient state
5	31	5/2007	Transient state
6	30	6/2007	Transient state
7	31	7/2007	Transient state
8	31	8/2007	Transient state
9	30	9/2007	Transient state
10	11	1/10/2007–11/10/2007	Transient state
11	20	12/10/2007–31/10/2007	Transient state
12	30	11/2007	Transient state
13	31	12/2007	Transient state

8.6. Mathematical Model Results

After the groundwater flow model was calibrated the water budget showed that Nestos River is the main contributor to the model, with a total of 27.61 MCM/a, which accounts 50.61% of the total inflows in the model (Figure 18). Inflows from the northern (GHB) boundary are calculated 3.26 MCM/a (5.98%), while water coming from precipitation recharge is 16.11 MCM/a and irrigation return flows water is 7.57 MCM/a, which correspond to 29.53% and 13.88% respectively. A small amount of water (0.1 MCM/a) also comes from the boundary representing the sea (CHD). The vast majority of outflows from the system come from the water that is pumped for irrigation, which is 50.46 MCM/a, representing 90.07% of the total outflows. This leaves only 5.02 MCM/a flowing towards the sea (8.95%), while smaller amount of water outflow towards the Nestos River boundary (0.29 MCM/a, 0.52% of outflows) and the Laspias drain boundary (0.26 MCM/a, 0.46% of outflows).

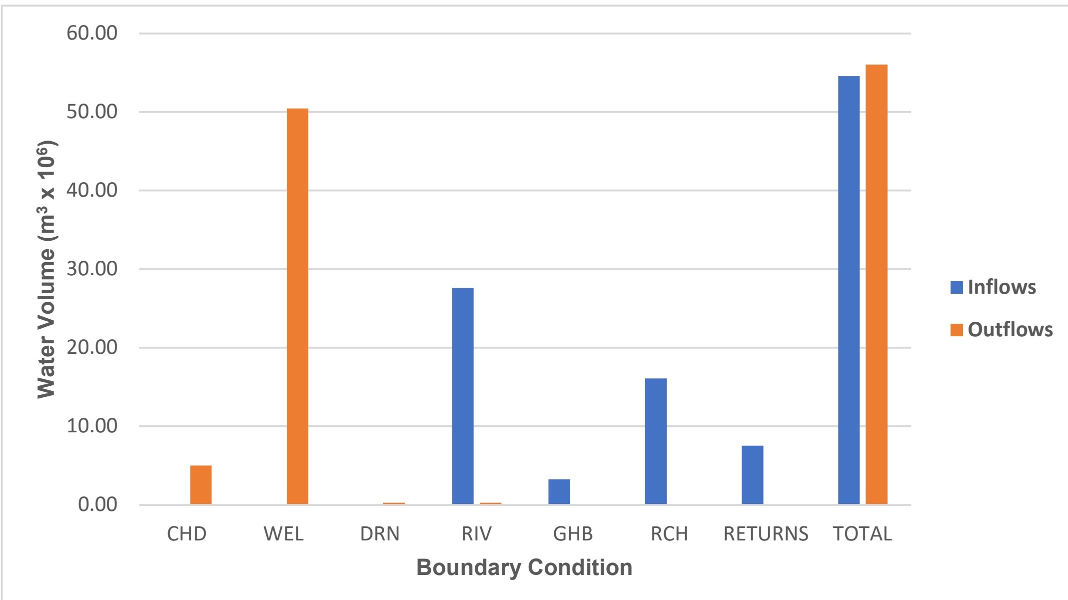

Figure 18. Groundwater budget components of the model.

The model results were evaluated using the statistical method of root mean square error, RMSE, following the mathematical expression below:

$$\mathrm{RMSE} = \sqrt{\frac{1}{n}\sum_{i=1}^{n}[(z_{hi} - h_i)]^2}$$

where z_{hi} are measurements of heads h_i at n locations and times.

Figure 19a–c, show the modelled against the measured values of hydraulic heads for the investigated aquifer, while Figure 20a–c, show the piezometric maps of modeled and measured groundwater levels within the study area. The above figures, show that the modeled hydraulic heads fit better with the measured ones for most of the model domain, apart from some specific parts within the coastal zone. The Figures 19a–c and 20a–c are representative for critical states of the aquifer during the model calibration i.e., (a) final time step of 1st stress period under steady state conditions, (b) final time step of 4th stress period under transient state conditions corresponding to the wet period prior irrigations, (c) 10th time step of 11th stress period under transient state conditions corresponding to the dry period posterior the irrigation period.

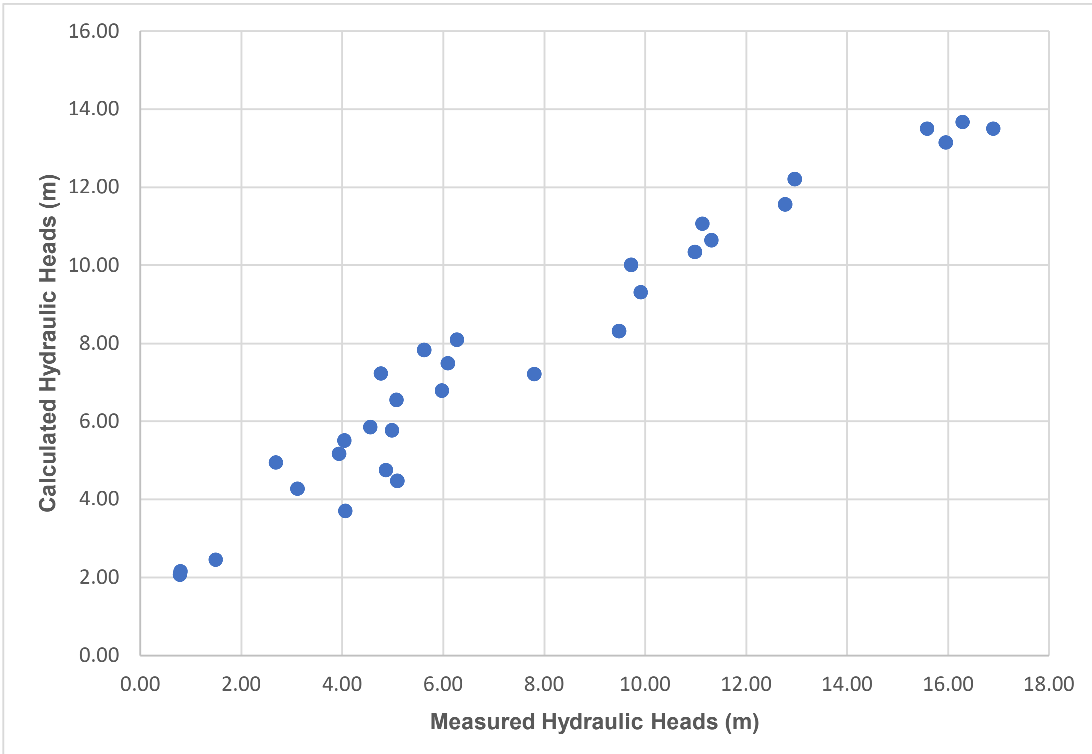
16.00
14.00
12.00
10.00
8.00
6.00
4.00
2.00
0.00
Calculated Hydraulic Heads (m)
0.00
2.00
4.00
6.00
8.00
10.00
12.00
14.00
16.00
18.00
Measured Hydraulic Heads (m)

(**a**)

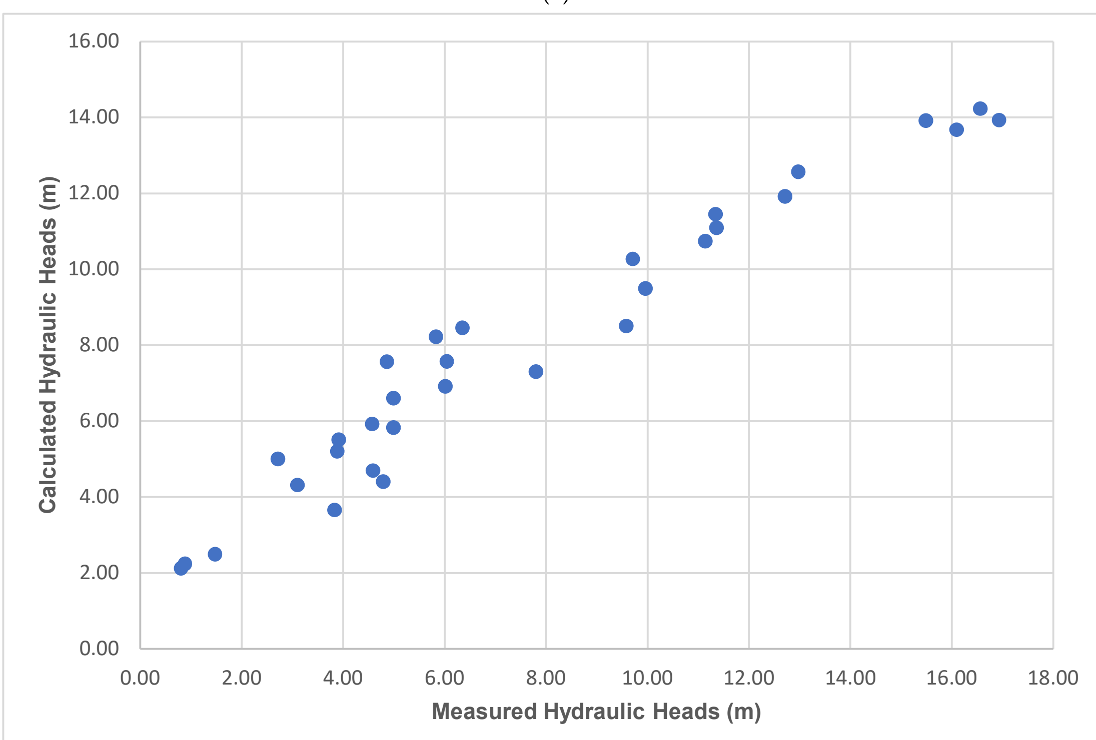
16.00
14.00
12.00
10.00
8.00
6.00
4.00
2.00
0.00
Calculated Hydraulic Heads (m)
0.00
2.00
4.00
6.00
8.00
10.00
12.00
14.00
16.00
18.00
Measured Hydraulic Heads (m)

(**b**)

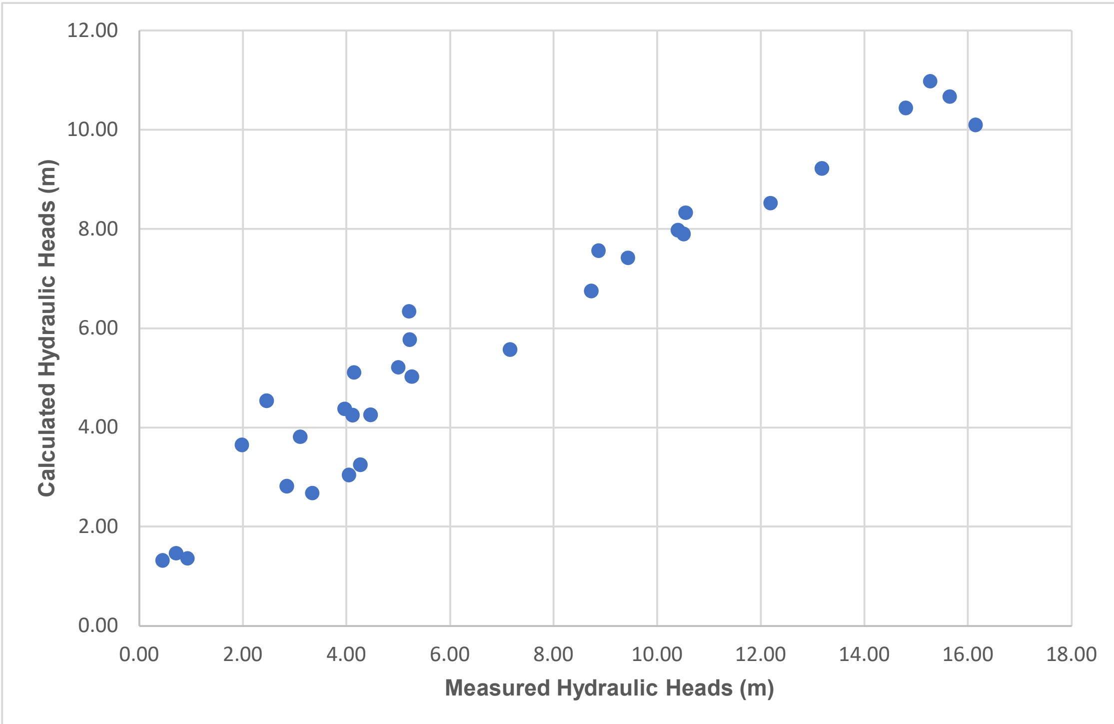

(**c**)

Figure 19. Calculated vs. measured hydraulic heads in critical stress periods and time steps: (**a**) final time step of 1st stress period under steady state conditions, (**b**) final time step of 4th stress period under transient state conditions corresponding to the wet period prior irrigations, (**c**) 10th time step of 11th stress period under transient state conditions corresponding to the dry period posterior the irrigation period.

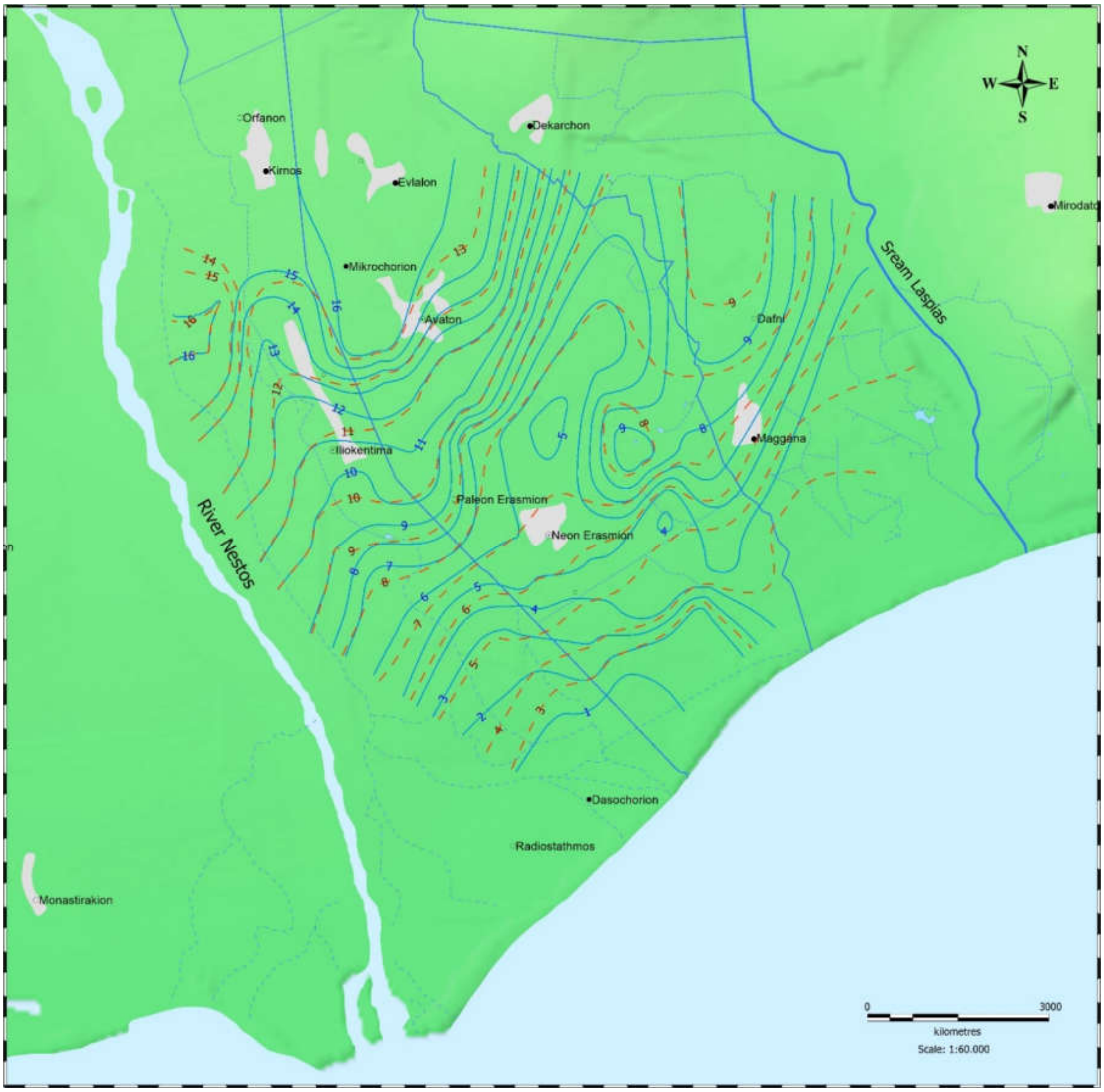

Orfanon
Kimos
Evlalon
Dekarchon
Mirodato
Mikrochorion
Avaton
Dafni
Maggana
Iliokentima
Paleon Erasmion
Neon Erasmion
Dasochorion
Radiostathmos
Monastirakion
River Nestos
Sream Laspias
N
S
W
E
0
3000
kilometres
Scale: 1:60.000

(**a**)

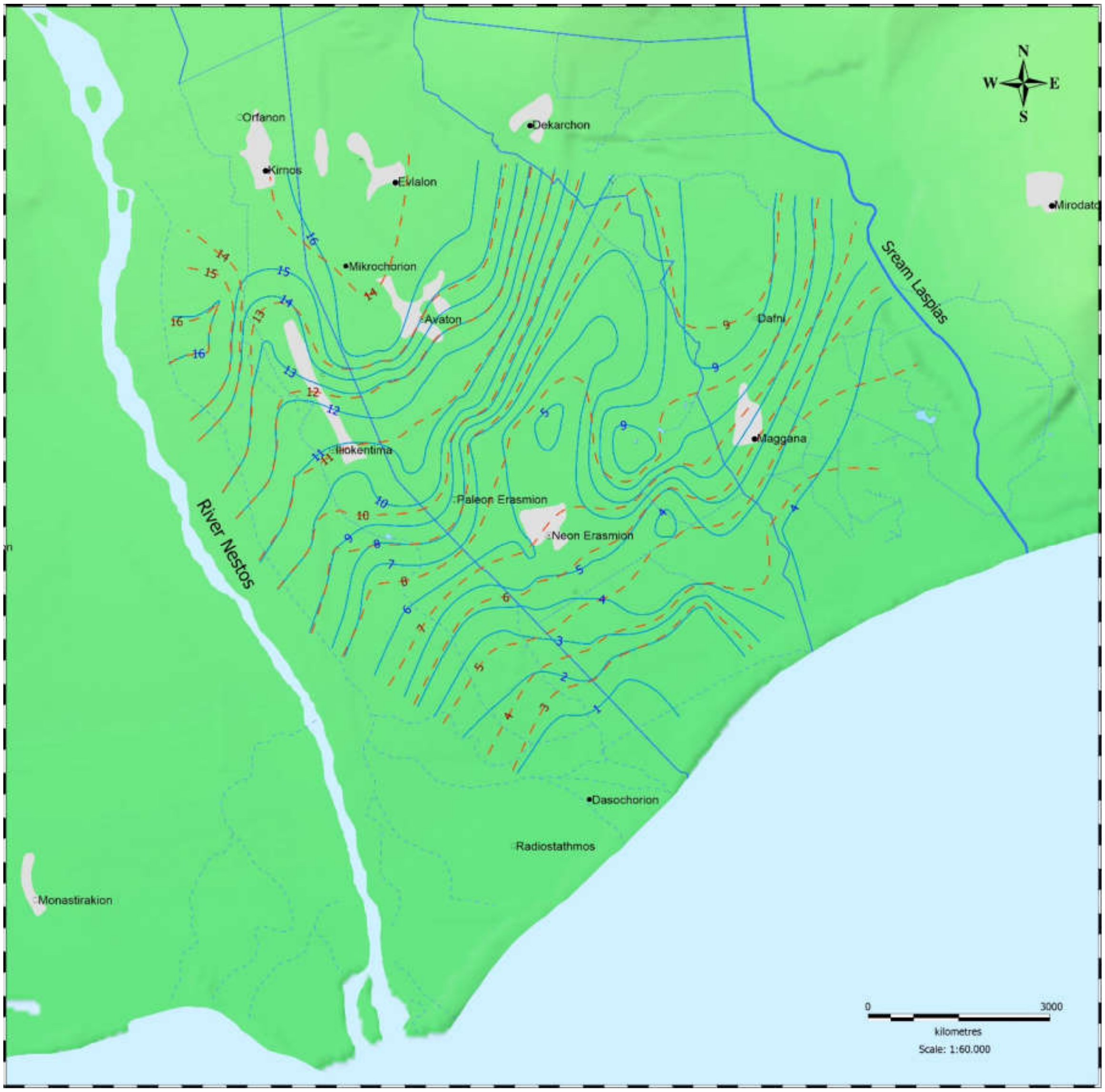
N
W
E
S
Orfanon
Kimos
Evlalon
Dekarchon
Mirodato
Mikrochorion
Avaton
Dafni
Sream Laspias
Maggana
Iliokentima
Paleon Erasmion
Neon Erasmion
River Nestos
Dasochorion
Radiostathmos
Monastirakion
0
3000
kilometres
Scale: 1:60.000

(**b**)

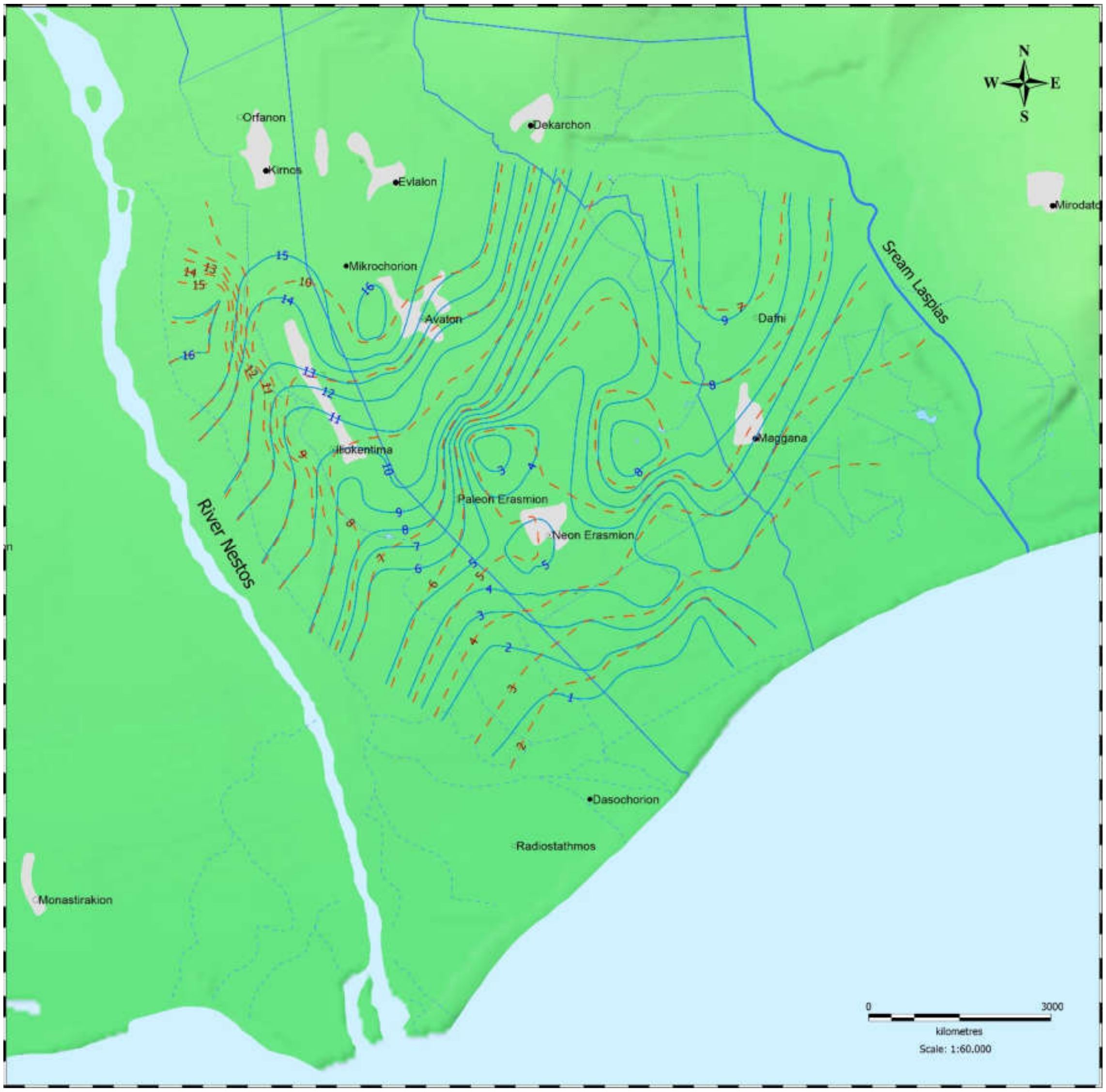

(**c**)

Figure 20. Calculated vs. measured piezometric map in critical stress periods and time steps: (**a**) final time step of 1st stress period under steady state conditions, (**b**) final time step of 4th stress period under transient state conditions corresponding to the wet period prior irrigations, (**c**) 10th time step of 11th stress period under transient state conditions corresponding to the dry period posterior the irrigation period.

9. Conclusions

The case study of the eastern delta plain of River Nestos (N. Greece) has played an important role to the economic development of the region. However, this was the reason for the quantitative and qualitative degradation of its phreatic and confined groundwater aquifer, after a long period of intense pumping conditions. Land reclamation through the construction of a network of drainage canals, aggravated the local piezometric conditions through lowering of the water table within the coastal part.

The research area is surrounded by Nestos river on the west and by the Aegean Sea on the south. The broader region morphology, on the south and south-east, is identified by low relief and some shallow pits, thus creating minor ponds, that are fragment of the eastern Nestos River delta wetland. The research area is mainly coved by clay, sandy clay, sand and in some cases pebbles. Nestos River stands dominant as the most significant surface water body of this region.

A large part of the wider area of the eastern Nestos delta is estimated as problematic because of its hydraulic linkage to the sea and also to the limited recharge of the groundwater and the overexploitation of the aquifers. These factors have contributed to the continuous salinization of groundwater and soils.

The research area is situated in holocene delta environment deposits with a thickness of some tens of meters built by River Nestos and sub-streams. These deposits consists of alternate clay, sand and silt layering, have resulted in a broad range of formational and depositional tasks, that produced a very diverse geological domain. In addition, due to delta marshes the existence of organic clay at some spot is identified. The advancement of the eastern Nestos delta in conjunction with flooding conditions has been contributory in shaping low potential aquifers in the research area.

In the research area ten (10) geoelectrical soundings were conducted, with the main target being to identify the stratigraphy of the region (Figure 1). This task was executed as stated by the Schlumberger method for measuring soil resistivity. The survey spots were determined so that they can cover parts of the research area where the stratigraphy was not well identified. The results of the geoelectrical soundings correlate directly with stratigraphy data.

Rainfall data from the area is analyzed in this manuscript, for the period 1966 to 2013, and the average monthly rainfall for the periods 1966–2012, 1985–2012, 1995–2012, 2000–2012 is presented. After processing of all the relevant diagrams of the preceding figures, useful outcomes were obtained.

Two hydrogeological systems are identified in the research area, which are situated within the quaternary coastal and alluvial deposits of the broader region [46]. The first hydrogeological system is consisted by of phreatic to semi-confined aquifers with a thickness of approximately 30 m. The main recharge of this hydrogeological system is mainly from precipitation and partly from nearby small streams and canals. The second deeper hydrogeological system of the study area, incorporates alternate confined aquifers with a thickness of approximately 200 m. Recharge of the second system derives partly from river Nestos infiltration through old buried river beds, and partly from lateral groundwater inflows originate from the neighboring hydrogeological basin of Vistonida lagoon.

Estimation of the groundwater hydraulic parameters of the research area aquifers after analyzing the pumping test data from 11 selected wells in the broader research area derived in values for [46]: (1) transmissivity (T), ranging from 4.0×10^{-4} to 1.1×10^{-2} m^2/sec, (2) storage coefficient (S), ranging from very low values to 10^{-3}, rendering the aquifers of the research area as mainly confined westward, and in several sites as semi-confined.

Chemical analyzes and in-situ measurements were performed for the needs of this research. The examined parameters were: Ca^{2+}, Mg^{2+}, Na^+, K^+, HCO_3^-, Cl^-, SO_4^{2-}, NO_3^-, NO_2^-, NH_4^+, PO_4^{3-}, SiO_2, Fe^{2+}, Mn^{2+}, alkalinity P, alkalinity M, hardness (permanent, non-permanent, total), pH, electrical conductivity (EC). From the analysis of Piper and Durov charts as well as the correlation plot of SO_4 + HCO_3 vs. Cl, obtained from 30 sample wells, it is concluded that the majority of the samples are in the range of conservative mixture between freshwater and saltwater, and some of the samples show significant salinity problems due to possible seawater intrusion.

Based on SAR, TDS, EC values and concentrations of Na^+, Cl^- and HCO_3^- of water samples in 2009 and 2013, the restriction level on use was estimated (DRU, degree of restriction on use) [59,60], and characterized [52,61]: (i) regarding salinity (affecting water for plant growth), as small to medium (SM) in the majority of samples, and as severe (S) in a few of them (4), (ii) regarding the permeability (affecting the rate of water infiltration in soil), as minimal (N), small and average (SM), (iii) regarding the specific ion toxicity (affecting sensitive plants), as minimal (N) to severe (S), with typical the surface irrigation where several samples of groundwater assessed as small to average degree (SM) in restriction on use (DRU).

The results for the isotope analysis reveal that the groundwater from of the study area is isotopically heavy. This can be seen from the plot of δD as a function of $\delta^{18}O$ (Figure

12), where most points fall close to the global meteoric water line (GMWL: $\delta^2H = 8\delta^{18}O + 10$) with heavier isotopic values. The plot shows a pattern of two clusters of points; one very close to GMWL and the other away from it. The former represents isotope results for the wells located to the east of the study area close to the Aegean Sea. This implies that the aquifer in the part of the study area is subjected to recharge mainly from the sea by seawater intrusion.

The synthesis of the above, in combination with existing data (geological, hydrological, meteorological etc.), provided the basis for the development of the conceptual model for the study area, prior the application of the mathematical model.

The study of the coastal aquifer of Nestos phreatic coastal aquifer involved also the development of a mathematical model for the simulation of groundwater flow. The applied numerical code is MODFLOW-2005, using the finite difference method and taking into account all the available hydrogeological information for the setting of the boundary conditions of the model. The model involved several packages (GHB, CHB, RIV, DRN, WEL, RCH, HOB) for the simulation of the relevant hydrological processes and stresses on the investigated aquifer, resulted in satisfactory results.

The application of the above, proved that the development of an accurate mathematical model strongly relies on a reliable conceptual model which in turn depends largely on a series of field and lab measurements usually involving time and economic costs. However, it was realized that the modeling efforts can seriously lowered when the conceptualization process is of high quality.

Author Contributions: Methodology, I.G.; software, I.G. and C.P.; validation, F.-K.P., I.D. and A.K.; formal analysis, I.G.; investigation, I.G.; data curation, I.G.; writing—original draft preparation, I.G. and A.K.; writing—review and editing, C.P., F.-K.P. and A.K.; visualization, I.G.; supervision, F.-K.P., I.D. and A.K. All authors have read and agreed to the published version of the manuscript.

Funding: This research received no external funding.

Institutional Review Board Statement: Not applicable.

Informed Consent Statement: Not applicable.

Data Availability Statement: Not applicable.

Conflicts of Interest: The authors declare no conflict of interest.

References

1. Park, Y.; Lee, J.-Y.; Kim, J.-H.; Song, S.-H. National scale evaluation of groundwater chemistry in Korea coastal aquifers: Evidences of seawater intrusion. *Environ. Earth Sci.* **2012**, *66*, 707–718.
2. Shi, L.; Jiao, J.J. Seawater intrusion and coastal aquifer management in China: A review. *Environ. Earth Sci.* **2014**, *72*, 2811–2819, doi:10.1007/s12665-014-3186-9.
3. Sophiya, M.S.; Syed, T.H. Assessment of vulnerability to seawater intrusion and potential remediation measures for coastal aquifers: A case study from eastern India. *Environ. Earth Sci.* **2013**, *70*, 1197–1209, doi:10.1007/s12665-012-2206-x.
4. Baharuddin, M.F.T.; Othman, A.R.; Taib, S.; Hashim, R.; Zainalabidin, M.H.; Radzuan, M.A. Evaluating freshwater lens morphology affected by seawater intrusion using chemistry-resistivity integrated technique: A case study of two different land covers in Carey Island, Malaysia. *Environ. Earth Sci.* **2012**, *69*, 2779–2797, doi:10.1007/s12665-012-2098-9.
5. Teng, Y.; Su, J.; Wang, J.; Dai, N.; Li, J.; Song, L.; Zuo, R. Soil microbial community response to seawater intrusion into coastal aquifer of Donghai Island, South China. *Environ. Earth Sci.* **2014**, *72*, 3329–3338, doi:10.1007/s12665-014-3236-3.
6. Mtoni, Y.; Mjemah, I.C.; Bakundukize, C.; Van Camp, M.; Martens, K.; Walraevens, K. Saltwater intrusion and nitrate pollution in the coastal aquifer of Dar es Salaam, Tanzania. *Environ. Earth Sci.* **2013**, *70*, 1091–1111, doi:10.1007/s12665-012-2197-7.
7. Chandrajith, R.; Chaturangani, D.; Abeykoon, S.; Barth, J.A.C.; Van Geldern, R.; Edirisinghe, E.A.N.V.; Dissanayake, C.B. Quantification of groundwater–seawater interaction in a coastal sandy aquifer system: A study from Panama, Sri Lanka. *Environ. Earth Sci.* **2013**, *72*, 867–877, doi:10.1007/s12665-013-3010-y.
8. Li, G.; Wang, X.; Meng, Z.; Zhao, H. Seawater inrush assessment based on hydrochemical analysis enhanced by hierarchy clustering in an undersea goldmine pit, China. *Environ. Earth Sci.* **2013**, *71*, 4977–4987, doi:10.1007/s12665-013-2888-8.
9. Kaya, M.A.; Özürlan, G.; Balkaya, Çağlayan Geoelectrical investigation of seawater intrusion in the coastal urban area of Çanakkale, NW Turkey. *Environ. Earth Sci.* **2014**, *73*, 1151–1160, doi:10.1007/s12665-014-3467-3.

10. Saidi, S.; Bouri, S.; Ben Dhia, H. Groundwater management based on GIS techniques, chemical indicators and vulnerability to seawater intrusion modelling: Application to the Mahdia–Ksour Essaf aquifer, Tunisia. *Environ. Earth Sci.* **2013**, *70*, 1551–1568, doi:10.1007/s12665-013-2241-2.
11. Manca, F.; Capelli, G.; Tuccimei, P. Sea salt aerosol groundwater salinization in the Litorale Romano Natural Reserve (Rome, Central Italy). *Environ. Earth Sci.* **2014**, *73*, 4179–4190, doi:10.1007/s12665-014-3704-9.
12. Rey, J.; Martínez, J.; Barberá, G.G.; García-Aróstegui, J.L.; García-Pintado, J.; Martínez-Vicente, D. Geophysical characterization of the complex dynamics of groundwater and seawater exchange in a highly stressed aquifer system linked to a coastal lagoon (SE Spain). *Environ. Earth Sci.* **2013**, *70*, 2271–2282, doi:10.1007/s12665-013-2472-2.
13. Ben Hamouda, M.F.; Tarhouni, J.; LeDuc, C.; Zouari, K. Understanding the origin of salinization of the Plio-quaternary eastern coastal aquifer of Cap Bon (Tunisia) using geochemical and isotope investigations. *Environ. Earth Sci.* **2010**, *63*, 889–901, doi:10.1007/s12665-010-0758-1.
14. Elewa, H.H.; Shohaib, R.E.; Qaddah, A.A.; Nousir, A.M. Determining groundwater protection zones for the Quaternary aquifer of northeastern Nile Delta using GIS-based vulnerability mapping. *Environ. Earth Sci.* **2013**, *68*, 313–331.
15. Terzić, J.; Peh, Z.; Marković, T. Hydrochemical properties of transition zone between fresh groundwater and seawater in karst environment of the Adriatic islands, Croatia. *Environ. Earth Sci.* **2010**, *59*, 1629–1642.
16. Trabelsi, R.; Abid, K.; Zouari, K.; Yahyaoui, H. Groundwater salinization processes in shallow coastal aquifer of Djeffara plain of Medenine, Southeastern Tunisia. *Environ. Earth Sci.* **2011**, *66*, 641–653, doi:10.1007/s12665-011-1273-8.
17. Kharroubi, A.; Tlahigue, F.; Agoubi, B.; Azri, C.; Bouri, S. Hydrochemical and statistical studies of the groundwater salinization in Mediterranean arid zones: Case of the Jerba coastal aquifer in southeast Tunisia. *Environ. Earth Sci.* **2012**, *67*, 2089–2100, doi:10.1007/s12665-012-1648-5.
18. Sdao, F.; Parisi, S.; Kalisperi, D.; Pascale, S.; Soupios, P.; Simantiris, N.L.; Kouli, M. Geochemistry and quality of the groundwater from the karstic and coastal aquifer of Geropotamos River Basin at north-central Crete, Greece. *Environ. Earth Sci.* **2012**, *67*, 1145–1153.
19. Özler, H.M. Carbonate weathering and connate seawater influencing karst groundwaters in the Gevas–Gurpinar–Güzelsu basins, Turkey. *Environ. Earth Sci.* **2010**, *61*, 323–340.
20. Ahmed, M.A.; Abdel Samie, S.G.; Badawy, H.A. Factors controlling mechanisms of groundwater salinization and hydrogeochemical processes in the Quaternary aquifer of the Eastern Nile Delta, Egypt. *Environ. Earth Sci.* **2013**, *68*, 369–394.
21. Cuoco, E.; Darrah, T.H.; Buono, G.; Eymold, W.K.; Tedesco, D. Differentiating natural and anthropogenic impacts on water quality in a hydrothermal coastal aquifer (Mondragone Plain, Southern Italy). *Environ. Earth Sci.* **2015**, *73*, 7115–7134, doi:10.1007/s12665-014-3892-3.
22. Yousif, M.; Bubenzer, O. An integrated approach for groundwater assessment at the Northwestern Coast of Egypt (Ras El Hekma area): Case study. *Environ. Earth Sci.* **2012**, *69*, 2227–2246, doi:10.1007/s12665-012-2052-x.
23. Manca, F.; Capelli, G.; La Vigna, F.; Mazza, R.; Pascarella, A. Wind-induced salt-wedge intrusion in the Tiber river mouth (Rome–Central Italy). *Environ. Earth Sci.* **2014**, *72*, 1083–1095, doi:10.1007/s12665-013-3024-5.
24. Güler, C. Site characterization and monitoring of natural attenuation indicator parameters in a fuel contaminated coastal aquifer: Karaduvar (Mersin, SE Turkey). *Environ. Earth Sci.* **2009**, *59*, 631–643, doi:10.1007/s12665-009-0060-2.
25. Chaaban, F.; Darwishe, H.; Louche, B.; Battiau-Queney, Y.; Masson, E.; El Khattabi, J.; Carlier, E. Geographical information system approach for environmental management in coastal area (Hardelot-Plage, France). *Environ. Earth Sci.* **2011**, *65*, 183–193, doi:10.1007/s12665-011-1080-2.
26. Carneiro, J.F.; Boughriba, M.; Correia, A.; Zarhloule, Y.; Rimi, A.; El Houadi, B. Evaluation of climate change effects in a coastal aquifer in Morocco using a density-dependent numerical model. *Environ. Earth Sci.* **2009**, *61*, 241–252, doi:10.1007/s12665-009-0339-3.
27. Tassy, A.; Maxwell, M.; Borgomano, J.; Arfib, B.; Fournier, F.; Gilli, E.; Guglielmi, Y. Electrical resistivity tomography (ERT) of a coastal carbonate aquifer (Port-Miou, SE France). *Environ. Earth Sci.* **2013**, *71*, 601–608, doi:10.1007/s12665-013-2802-4.
28. Pezzetta, E.; Lutman, A.; Martinuzzi, I.; Viola, C.; Bernardis, G.; Fuccaro, V. Iron concentrations in selected groundwater samples from the lower Friulian Plain, northeast Italy: Importance of salinity. *Environ. Earth Sci.* **2010**, *62*, 377–391, doi:10.1007/s12665-010-0533-3.
29. Gaaloul, N.; Pliakas, F.; Kallioras, A.; Schuth, C.; Marinos, P. Simulation of seawater intrusion in coastal aquifers: Forty five-years exploitation in an eastern coast aquifer in NE Tunisia. *Open Hydrol. J.* **2012**, *6*, 31–44.
30. Diamantis, J.; Petalas, C. Sea water Intrusion into Coastal aquifers of Thrace and its impact on the environment. *Toxicol. Environ. Chem.* 1989, *20–21*, 291–305.
31. Gkiougkis, I.; Kallioras, A.; Pliakas, F.; Pechtelidis, A.; Diamantis, V.; Ziogas, A.; Dafnis, I.; Diamantis, I. Assessment of soil salinization at the eastern Nestos River Delta, N.E. Greece. *Catena* **2015**, *128*, 238–251, doi:10.1016/j.catena.2014.06.024.
32. Kallioras, A.; Pliakas, F.; Diamantis, I.; Emmanouil, M. Application of Geographical Information Systems (GIS) for the management of coastal aquifers subjected to seawater intrusion. *J. Environ. Sci. Health Part. A Toxic Hazard. Subst. Environ. Eng.* **2006**, *A41*, 2027–2044.
33. Kallioras, A.; Pliakas, F.; Diamantis, I. Conceptual model of a coastal aquifer system in northern Greece and assessment of saline vulnerability due to seawater intrusion conditions. *Environ. Geol.* **2006**, *51*, 349–361.
34. Kallioras, A.; Pliakas, F.; Diamantis, I. Simulation of groundwater flow in a sedimentary aquifer system subjected to overexploitation. *Water Air Soil Pollut.* **2010**, *211*, 177–201.

35. Kallioras, A.; Pliakas, F.; Diamantis, I.; Kallergis, G. SWOT analysis in groundwater resources management of coastal aquifers: A case study from Greece. *Water Int.* **2010**, *35*, 425–441, doi:10.1080/02508060.2010.508929.
36. Lambrakis, N.; Kallergis, G. Reaction of subsurface coastal aquifers to climate and land use changes in Greece: Modelling of groundwater refreshening patterns under natural recharge conditions. *J. Hydrol.* **2001**, *245*, 19–31, doi:10.1016/s0022-1694(01)00334-1.
37. Maramathas, A.; Pergialiotis, P.; Gialamas, I. Contribution to the identification of the sea intrusion mechanism of brackish karst springs. *Hydrogeol. J.* **2005**, *14*, 657–662, doi:10.1007/s10040-005-0466-1.
38. Panagopoulos, G.; Lambrakis, N.; Tsolis-Katagas, P.; Panagoulis, D. Cation exchange processes and human activities in unconfined aquifers. *Environmental Geology* **2004**, *46*, 542–552.
39. Petalas, C.P.; Diamantis, I.B. Origin and distribution of saline groundwaters in the upper Miocene aquifer system, coastal Rhodope area, northeastern Greece. *Hydrogeol. J.* **1999**, *7*, 305–316, doi:10.1007/s100400050204.
40. Recinos, N.; Kallioras, A.; Pliakas, F.; Schuth, C. Application of GALDIT index to assess the intrinsic vulnerability to seawater intrusion of coastal granular aquifers. *Environ. Earth Sci.* **2015**, *73*, 1017–1032, doi:10.1007/s12665-014-3452-x.
41. Rousakis, G.; Karageorgis, A.P.; Georgiou, P. Geological structure and seabed morphology of the Stoupa submarine groundwater discharge system, Messinia, Greece. *Environ. Earth Sci.* **2014**, *71*, 5059–5069.
42. Boughriba, M.; Jilali, A. Climate change and modeling of an unconfined aquifer: The Triffa plain, Morocco. *Environ. Dev. Sustain.* **2017**, *20*, 2009–2026, doi:10.1007/s10668-017-9974-0.
43. Matiatos, I.; Paraskevopoulou, V.; Lazogiannis, K.; Botsou, F.; Dassenakis, M.; Ghionis, G.; Alexopoulos, J.D.; Poulos, S.E. Surface–ground water interactions and hydrogeochemical evolution in a fluvio-deltaic setting: The case study of the Pinios River delta. *J. Hydrol.* **2018**, *561*, 236–249, doi:10.1016/j.jhydrol.2018.03.067.
44. Polemio, M.; Lonigro, T. Trends in climate, short-duration rainfall, and damaging hydrogeological events (Apulia, Southern Italy). *Nat. Hazards* **2015**, *75*, 515–540, doi:10.1007/s11069-014-1333-y.
45. Vespasiano, G.; Cianflone, G.; Romanazzi, A.; Apollaro, C.; Dominici, R.; Polemio, M.; De Rosa, R. A multidisciplinary approach for sustainable management of a complex coastal plain: The case of Sibari Plain (Southern Italy). *Mar. Pet. Geol.* **2019**, *109*, 740–759, doi:10.1016/j.marpetgeo.2019.06.031.
46. Sakkas, I.; Diamantis, I.; Pliakas, F. *Groundwater Artificial Recharge Study of Xanthi—Rhodopi aquifers (in Thrace, Greece)*; Greek Ministry of Agriculture Research Project, Final Report; Sections of Geotechnical Engineering and Hydraulics of the Civil Engineering Department of Democritus University of Thrace: Xanthi, Greece, 1998. (In Greek)
47. Boskidis, I.; Pisinaras, V.; Petalas, C.; Tsihrintzis, V.A. Monitoring and modeling of two alluvial aquifers in lower Nestos river basin, Northern Greece. *J. Environ. Sci. Heal. Part A* **2012**, *47*, 1849–1868, doi:10.1080/10934529.2012.689552.
48. Petalas, C.; Pliakas, F.; Diamantis, I.; Kallioras, A. Development of an integrated conceptual model for the rational management of the transboundary Nestos River, Greece. *Environ. Earth Sci.* **2005**, *48*, 941–954, doi:10.1007/s00254-005-0032-0.
49. Pedreira, R.; Kallioras, A.; Pliakas, F.; Gkiougkis, I.; Schuth, C. Groundwater vulnerability assessment of a coastal aquifer system at River Nestos eastern Delta, Greece. *Environ. Earth Sci.* **2015**, *73*, 6387–6415, doi:10.1007/s12665-014-3864-7.
50. ASCE. *Ground Water Management*, 3rd ed.; ASCE Manuals and Reports on Engineering Practice No 40; American Society of Civil Engineers: New York, NY, USA, 1987.
51. Kallergis, G. *Applied—Environmental Hydrogeology, Volume B*; TCG: Athens, Greece, 2000; p. 345. (In Greek)
52. Pliakas, F.; Diamantis, I.; Gkiougkis, I.; Mimidis, K.; Tzevelekis, T.; Bellos, K. *Water Resources Management at the Wider Region of the R. Nestos Eastern Delta for Optimal Meet of Irrigation Needs and the Improvement of Groundwater Quality*; Research Report on Behalf of Administrative Region of East Macedonia and Thrace—Regional Unit of Xanthi: Xanthi, Greece, 2014; p. 182. (In Greek)
53. Rainwater, F.H.; Thatcher, L.L. Methods for collection and analysis of water samples. In *Methods for Collection and Analysis of Water Samples*; US Geological Survey: Reston, WI, USA, 1960; p. 301.
54. American Public Health Association. *Standard Methods for Examination of Water and Wastewater*, 20th ed.; Clescerl, L., Greenberg, A., Eaton, A., Eds; American Public Health Association: Washington, DC, USA, 1999, p. 1325.
55. Ayers, R.S. Quality of water for irrigation. In Proceeding of the Irrigation and Drainage Division, Specialty Conference, ASCE, Logan, Utah, 13–15 August 1975; pp. 24–56.
56. Richards, L.A. Diagnosis and Improvement of Saline and Alkali Soils. *Soil Sci.* **1954**, *78*, 154, doi:10.1097/00010694-195408000-00012.
57. Wilcox, L.V. *Classification and Use of Irrigation Waters*; Circular No. 969; USDA: Washington, DC, USA, 1955.
58. Revelle, R. Criteria for recognition of the sea water in ground-waters. *Trans. Am. Geophys. Union* **1941**, *22*, 593–597, doi:10.1029/tr022i003p00593.
59. Asano, T.; Pettygrove, G.S. Using reclaimed municipal wastewater for irrigation. *Calif. Agric.* **1987**, *41*, 15–18, doi:10.3733/ca.v041n03p15.
60. Roscoe Moss Company. *Handbook of Ground Water Development*; John Wiley & Sons: Hoboken, NJ, USA, 1990; p. 493.
61. Preka, I. Assessment of the hydrogeological regime of an aquifer system at the eastern R. Nestos Delta. Master's Thesis, MSc Hydraulic Engineering. Department of Civil Engineering, Democritus University of Thrace, Xanthi, Greece, 2009. (In Greek)
62. Harbaugh, A.W.; Langevin, C.D.; Hughes, J.D.; Niswonger, R.N.; Konikow, L.F. *MODFLOW-2005 Version 1.12.00, the U.S. Geological Survey Modular Groundwater Model*; U.S. Geological Survey Software Release; U.S. Geological Survey: Reston, WI, USA, 2017.

63. Harbaugh, A.W. *MODFLOW-2005, the U.S. Geological Survey Modular Ground-Water Model—the Ground-Water Flow Process*; U.S. Geological Survey Techniques and Methods 6-A16; U.S. Geological Survey: Reston, WI, USA, 2005.
64. McDonald, M.; Harbaugh, A.W. A Modular Three-Dimensional Finite Difference Ground-Water Flow Model. In *Techniques of Water-Resources Investigations*; Book 6; U.S. Geological Survey: Reston, WI, USA, 1988; p. 588.